Received: 4 April 2022 | Revised: 13 July 2022 | Accepted: 12 September 2022

DOI: 10.1002/cta.3452

WILEY

ORIGINAL PAPER

A novel scan pattern for reconfiguration of partially shaded photovoltaic arrays for maximum power extraction

Rayappa David Amar Raj | **Kanasottu Anil Naik**

Department of Electrical Engineering, National Institute of Technology, Warangal, Telangana, India

Correspondence
Rayappa David Amar Raj, Department of Electrical Engineering, National Institute of Technology, Warangal, Telangana, India.
Email: dtcdavid2k15@gmail.com

Abstract

Reconfiguration plays an indispensable role in augmenting the output of the photovoltaic (PV) array under partial shading conditions. Various reconfiguration schemes have been proposed in the literature to disperse the shade in partially shaded PV arrays. Nevertheless, most of these schemes can be employed only for less-rated arrays, are not compatible with all array sizes, fails in effective shade dispersion over the entire array, and so forth. To overcome these shortcomings, a calligraphy-based diagonal scan pattern is proposed to reconfigure the PV array to improve the row currents of the PV array thereby reducing the mismatch between them. The superiority of the proposed scheme is examined by comparing it with conventional Series-Parallel, Total-Cross-Tied, and the existing image processing based-Chaotic Baker Map, Odd-Even, and Odd-Even-Prime configurations. Besides, the system is extensively studied for various symmetrical 9×9, 8×8, 4×4, and unsymmetrical 8×6 PV arrays under 34 distinct shading cases with various performance indices. An experimental laboratory prototype model of a 4×4 PV array reconfiguration system is developed and studied under distinct shading conditions. Subsequently, an inclusive economic analysis is also conducted, and it is noted that there is a notable enhancement in electricity units and revenue generation by executing the proposed reconfiguration scheme.

KEYWORDS

calligraphy, diagonal scan, partial shading, photovoltaic array, reconfiguration, shade dispersal

1 | INTRODUCTION

The phenomenon of shading considerably reduces the photovoltaic (PV) array output and further leads to the formation of hotspots in the array. These hotspots create serious fire hazards and eventually damages the module.[1] So, a bypass diode is connected across the module for safety purposes. These diodes bypass the current under partial shading (PS) conditions.[2] Nevertheless, installing the bypass diodes stimulates several peaks in the Power-Voltage (P-V) and Current–Voltage (I-V) characteristics of an array. Further, the maximum power point tracking (MPPT) controllers are also considered to be a better solution for the PS problem. These controllers are installed in the subarrays of the system to lessen the impacts of shading and they require complex power converters and also efficient control algorithms for successful operation.[3] Despite its effectiveness in tracking the global maximum power (GMP) during shading, employing these controllers in the system raises the complexity and overall cost of the system. Furthermore, to extract

the output beyond what is solely obtained by MPPT trackers, the PV array reconfiguration is held as the foremost alternative.[4]

Broadly, the reconfiguration strategies are classified as static and dynamic strategies. The literature review of some distinguished dynamic reconfiguration strategies is as follows: Varma et al.[5] proposed a dynamic reconfiguration algorithm based on equalizing the irradiations of all the rows of an array and tested it for various PS conditions. This scheme employs a switching matrix that dynamically remodels the configuration of PV modules in an array. Karmakar and Karmakar[6] proposed and experimentally verified an enhanced dynamic reconfiguration technique employing a current-injection approach. By executing this technique, the multiple power peaks (MPPs) are considerably reduced in the array characteristics. In Babu et al.,[7] an evolutionary algorithm-based particle swarm optimization strategy is exercised to disperse the shade of a 9×9 PV array under various PS patterns, thereby mitigating the mismatch losses. Sanseverino et al.[8] employed a Munkres algorithm and dynamic programming for optimal reconfiguration of the PV array. Under partial shading scenarios, a new reconfiguration approach based on fuzzy logic (FL) is evaluated in Bouselham et al.[9] Additionally, an iterative least square-based irradiance estimator has been developed by the authors to minimize the dynamic PV array's investment cost. Very recently, a novel optimal mileage-based[10] and socio-inspired democratic political[11] approaches-based array reconfigurations are developed to dynamically reconfigure the array. To improve the reliability of PV modules, an automated reconfiguration technique is proposed in Yadav et al.[12] to evade the reverse breakdown and hotspots formation. Based on the type of shading pattern, the algorithm automatically switches to different array configurations to mitigate mismatch. Employing this scheme enhances the reliability of the PV array in 82% of the cases. However, the practical feasibility of this technique is challenging as it requires numerous switches, sensors, and training a large set of data. The dynamic reconfiguration strategies maximize the output under PS; nevertheless, they necessitate numerous current and voltage sensors, well-organized monitoring units, several complicated switches, complex algorithms to govern these switches, complicated controlling units, and effective driver circuitry, which increases the system complexity and cost. To dynamically reconfigure a 9×9 PV array for effective shade dispersion, the number of switches required is 1384.[13]

So, to evade the above-mentioned drawbacks of dynamic reconfiguration techniques, static reconfiguration techniques are preferred. Rani et al.[14] proposed a Sudoku puzzle-based approach for reconfiguring a 9×9 PV array. An increased shade dispersal compared to that of the Sudoku technique is achieved by an Optimal-Sudoku reconfiguration strategy.[15] To minimize the row currents mismatch in a PV array, Tatabhatla et al.[16] introduced an arrow Sudoku puzzle-based array reconfiguration for a small 6×6 PV array and tested it under various progressive shading conditions. However, these Sudoku-based techniques cannot be employed for asymmetric array sizes. Further, the major disadvantage with these Sudoku-based techniques is that there exist numerous puzzle patterns and obtaining the optimized Sudoku pattern is a great challenge. In addition to this, the effective shading dispersion in all the PS cases also cannot be assured. In Satpathy et al.,[17,18] novel shade dispersion approaches are proposed to mitigate the row current mismatch by interconnecting the panels in a predefined configuration. Employing the shift-based approaches to the PV array topologies,[19] the power production has been maximized under shading conditions. A static reconfiguration scheme based on the Lo Shu magic square is exercised for shade dispersal to enhance the GMP under PS.[20]

To avoid the complexity involved in the dynamic reconfiguration process and for obtaining the smooth PV array characteristics by effective shadow distribution, a fixed reconfiguration technique-based competence square[21] strategy have been proposed. To reduce the number of module interconnection ties necessitated, Ramesh et al.[22] proposed a triple tied (TT) array configuration scheme. Despite the ability of this scheme to reduce the interconnection ties, under some shading conditions, it is even inferior to total-cross-tied (TCT) configuration in its performance. Almost a balanced dispersal of shaded modules in various rows has been achieved in Madhanmohan et al.[23] by employing the diagonally distributed-TCT (D-TCT) reconfiguration procedure for a simple 4×4 PV array. Satpathy and Sharma[24] mitigated the effects of PS via one-time electrical reconfiguration of solar PV array of various standard and hybrid configurations such as Series-Parallel, Total Cross Tied, and Bridge Linked. To decrease mismatch power loss under diverse partial shade conditions, a new Magic-Square approach based static PV reconfiguration technique is proposed.[25] However, it cannot be applicable to all symmetrical and unsymmetrical arrays.

It is inferred that the static reconfiguration strategies are simple, economical, and competent. By employing some of the above-mentioned reconfiguration strategies, the first column elements remain unchanged, and hence if the shade occurs in the first column, it cannot be dispersed and renders a suboptimal solution for shading issues. Further, very few of these strategies are compatible with large-rated systems. So, developing an optimal reconfiguration of large-rated PV arrays for efficient shade dispersal continues as a substantial research gap. To disperse the shade in all the rows and columns, an innovative and efficient image processing-based PV array reconfiguration procedure designed by the

Chaotic Baker Map (CB) has been proposed[26] for an 8 × 8 PV arrays. This technique outperformed all the conventional array configurations and yields maximum power output by abating the mismatch in the row currents thereby reducing the PS loss. Despite its superior performance compared to conventional configurations, the CB technique has the following main shortcomings: (a) Incompetent shade dispersal over the entire PV array and (b) incompatibility with the un-symmetrical PV array size. The effect of irregular shading by nearby buildings and clouds on conventional and hybrid roof-top PV array configurations is investigated in Satpathy et al.[27] Recently, a modified Sudoku puzzle-based fixed reconfiguration approach is proposed in Rajani and Ramesh[28] to alleviate the shading losses; however, this technique cannot be scalable to all array sizes.

Very recently, a Chinese magic square-based physical relocation of panels[29] is proposed to disperse the shade to mitigate the shading impacts whose performance has been compared with the existing total-cross-tied configuration and distinct variants of the Sudoku-based techniques. However, the major setbacks of this technique are, it is not compatible with unsymmetrical arrays and, moreover, the power enhancement is also very less compared to Sudoku techniques. Another variant of the Sudoku puzzle named complementary SuDoKu is employed in Ye et al.[30] to relocate the panels for effective shade dispersal. The GMP enhancement with this technique is remarkably low compared to existing techniques. Besides, this technique is not compatible with unsymmetrical arrays. An AdDoKu pattern strategy for PV panels arrangement in a TCT configured array is introduced in Anjum et al.[31] without altering the electrical circuitry. It exhibits a power enhancement of 0.34%, 11.66%, 30.15%, and 28.76% under various shading cases. Notwithstanding, this approach cannot be compatible with unsymmetrical arrays. For increasing the power production of PV arrays during PS, a novel voltage equalization method based on the integration of TCT configuration design and switching capacitor approach is proposed.

A novel sequence-based interconnection algorithm for PV modules of a TCT configuration is introduced in Rakesh et al.[32] to alleviate the mismatch and wiring losses by using two improvised magic techniques. Nevertheless, complexity in the implementation of this technique increases with the PV array sizing. A static reconfiguration approach based on arithmetic sequence pattern (ASP) has been experimented on a 6 × 6 PV array.[33] But this technique is tested only under a square type of shading, which is insufficient to confirm the effectiveness of the technique. Moreover, the authors fail to demonstrate the compatibility of ASP for unsymmetrical PV arrays. To reconfigure the unsymmetrical PV arrays, an odd-even (OE) pattern-based scheme is introduced in Yadav et al.[34] to disperse the shade. An improvised version of the odd-even pattern named the odd-even-prime (OEP) pattern[35] is employed recently to relocate the panels physically of a TCT-configured PV array. A new prime numbers pattern-based arrangement of PV panels is proposed in Rezazadeh et al.[36] to maximize the output under PSC. The efficacy of this approach is examined under five distinct shading cases for 9 × 9 and 23 × 23 array orders. The power enhancement is in the range of 7–8% for the considered shading cases. Despite its scalability to all arrays, it performs inferior shade dispersal especially under diagonal shading resulting in suboptimal solution. Therefore, in this paper, a highly efficient calligraphy-based diagonal scan (DS) method is proposed to meet all the above-addressed shortcomings. The major contributions of the proposed work are as follows:

- As opposed to many existing static reconfiguration approaches,[14–26,28–33] the proposed technique is compatible for both symmetrical and un-symmetrical PV arrays (e.g., 5× 5, 7 × 9, 10 × 10, and 13 × 19), and further, it disperses the shade over the entire PV array. The compatibility and performance of the proposed DS are tested and analyzed for various symmetrical 9 × 9, 8 × 8, 4 × 4, and asymmetric 8 × 6 PV arrays.
- The proposed configuration is extensively analyzed with eight performance indices under 34 distinct nonuniform and uniform shading conditions.
- The effectiveness of the proposed configuration is compared with the conventional SP, TCT, and recently proposed Chaotic Baker Map,[26] Odd-Even,[34] and Odd-Even-Prime[35] configurations.
- A detailed analysis of row-current computations of various configurations under distinct shading conditions has been presented.
- For practical realization, the effect of temperature variation (with diverse temperature levels 25°C, 30°C, and 35°C) on various array configurations is also considered.
- An experimental laboratory prototype model of a 4 × 4 PV array reconfiguration system is developed and studied under distinct shading conditions.
- A qualitative comparative assessment of diverse aspects of the proposed configuration with the existing ones is detailed.
- A comprehensive economic analysis is also presented to demonstrate the monetary benefits associated with the proposed configuration.

2 | MODELING OF SOLAR PV ARRAY

The PV array comprises numerous PV modules connected in series–parallel, in which an individual module can be assembled with numerous PV cells in series–parallel. In the literature, various procedures for modeling a solar PV cell are published such as one-diode model, two-diode model, and three-diode models. Due to its simplicity, a one-diode equivalent circuit model is used in this analysis as shown in Figure 1A.

According to Kirchhoff's current law (KCL), the solar cell current is given as follows:

$$I_{PV\_cell} = I_{L\_cell} - I_d - I_{\text{sh}} \tag{1}$$

where I_{pv_cell} is the PV cell current, I_{L_cell} denotes light-produced current of PV cell, I_d denotes the diode current, and I_{sh} denotes shunt resistance current. By substituting I_{sh} and I_d in Equation (1), the cell current[37] can be computed as given

$$I_{PV\_cell} = I_{L\_cell} - I_0\left[\exp\left(q\frac{V_{cell}+I_{cell}R_{se}}{b\sigma T_c}-1\right)\right] - \frac{V_{cell}+I_{cell}R_{se}}{R_{sh}} \tag{2}$$

where I_o denotes diode saturation current, q denotes electron charge, V_{cell} denotes PV cell voltage, σ denotes ideality factor, T_c denotes operating temperature, b denotes Boltzmann's constant, R_{se} denotes PV cell series resistance, R_{sh} denotes shunt resistance. By considering a PV module comprising n_s series-connected cells, then the module current is given as

$$I_m = I_L - I_0\left[\exp\left(q\frac{V_m+I_mR_s}{n_sb\sigma T_c}-1\right)\right] - \frac{V_m+I_mR_{SE}}{R_{SH}} \tag{3}$$

where I_m denotes PV module current, q denotes electron charge, V_m denotes PV module voltage, R_{SE} denotes PV module series resistance, R_{SH} denotes PV module shunt resistance, and I_L denotes the light-produced current of PV module, which is computed as given

$$\mathrm{I_L} = \frac{\mathrm{G}}{\mathrm{G_0}}[\mathrm{I_{L\_STC}} + \mathrm{K_{sc}}(\mathrm{T_c} - \mathrm{T_0})] \tag{4}$$

where G denotes the actual irradiation, G_0 denotes standard irradiation, I_{L_STC} denotes PV module's light-produced current under the standard test condition (STC), K_{sc} denotes short-circuit current temperature coefficient factor, T_0 denotes standard operating temperature. The PV array consisting of $N_s \times N_p$ modules is shown in Figure 1B. Depending on the PV module output current as mentioned in Equation (3), the total PV array current is written as follows:

$$I_a = N_pI_L - N_pI_0\left[\exp\left(q\frac{V_a+\frac{N_s}{N_p}I_aR_s}{N_sn_sb\sigma T_c}-1\right)\right] - \left[\frac{V_a+\frac{N_s}{N_p}I_aR_s}{\frac{N_s}{N_p}R_{SH}}\right] \tag{5}$$

where V_a denotes array output voltage, I_a denotes array output current.

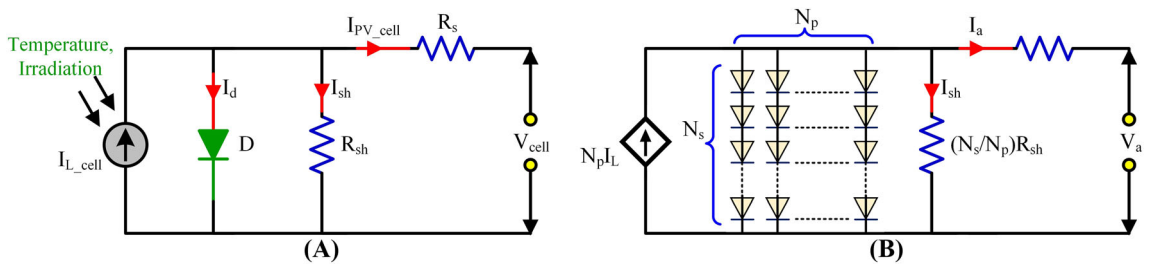

FIGURE 1 (A) Equivalent circuit of a PV cell, (B) equivalent circuit of PV array (with ns × np modules)

3 | STANDARD PV ARRAY CONFIGURATIONS

The various traditional array configurations described in the literature are Series–Parallel, Bridge-linked, Honey-Comb, and Total-Cross-Tied.[38] Among all the available traditional configurations, the Total-Cross-Tied (TCT) configuration which is shown in Figure 2D has superior performance due to the reasons listed as follows: enhanced GMP, improved array characteristics, greater output, and decreased mismatch losses during PS.[39] Notwithstanding its effectiveness over other configurations, during PS conditions, the TCT has the main shortcoming as it fails to dispense the shade and thus results in significant curtailment of output. Hence, there is a dire requirement for an optimal array reconfiguration for effective dispersal of shade under PS.

4 | PROPOSED METHODOLOGY

To obtain effective dispersal of shade through reconfiguration, a calligraphy-based DS pattern is employed as follows:

4.1 | Scan pattern

Generally, an image is considered to be a matrix constituted of many pixels. In the process of image encryption, these pixel coordinates (positions) are highly scrambled to obtain better security of the image.[40] The scan patterns are the commonly used techniques in image encryption to rearrange the pixel coordinates of the original image by employing the pixel permutation process. The scan pattern[41] is further described as scanning of a 2D array where every cell in the array is accessed by only one time. Some of the basic scan patterns[41] that are commonly employed to transfer the pixel coordinates of an image for encryption are shown in Figure 3A–D. From the scan patterns, the DS is observed to provide the best-randomized solution for rearranging the matrix coordinates when compared to other scanning patterns and thus, it is employed in the present work to disperse the shade in the PV array. In this paper, a diagonal scanning approach along with the abovementioned calligraphy scanning is employed to permute the pixel coordinates in an image.

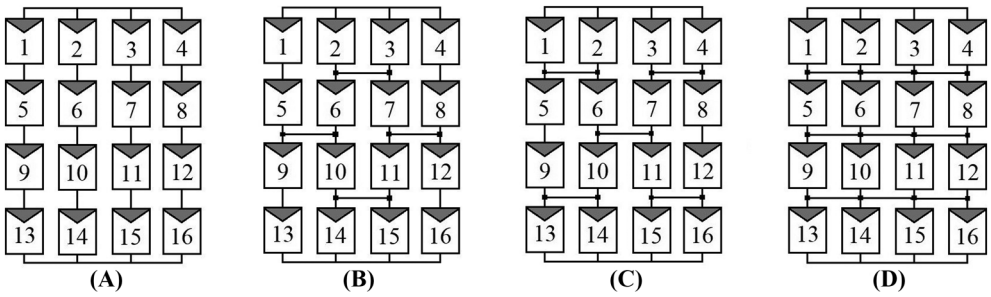

FIGURE 2 (A) Series-Parallel, (B) Honey-Comb, (C) Bridge-linked, and (D) Total-Cross-Tied TCT configurations

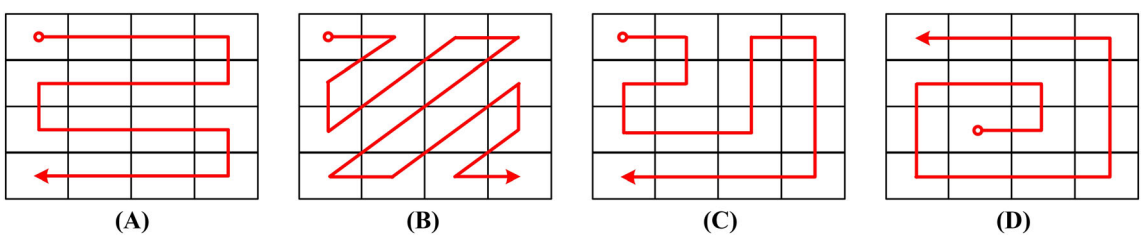

FIGURE 3 (A) Raster scan, (B) diagonal scan, (C) orthogonal scan (D) spiral scan

4.2 | Correlation between adjacent pixels

In the digital image, the correlation between the adjacent pixels is extremely high. To achieve better security, the image is generally applied with efficient image encryption techniques where the correlation between the adjacent pixels is highly reduced in order to be immune to various attacks. In ideal conditions, the correlation between adjacent pixels of an encrypted image should be zero. Generally, the effectiveness of any image encryption technique is decided by the correlation coefficient. The lower the correlation coefficient, the better the image encryption strategy. The correlation coefficient between the adjacent pixels of an encrypted image[42] can be estimated as follows:

$$\left.\begin{aligned} r_{xy} &= \frac{\mathrm{cov}(x,y)}{\sqrt{D(x)}\sqrt{D(y)}} \\ E(x) &= \frac{1}{N}\sum_{i=1}^{N}(x_i) \\ D(x) &= \frac{1}{N}\sum_{i=1}^{N}((x_i - E(x))^2 \\ \mathrm{cov}(x,y) &= \frac{1}{N}\sum_{i=1}^{N}((x_i - E(x)(y_i - E(y)) \end{aligned}\right\} \tag{6}$$

where r_{xy} is the correlation coefficient whose value is within ±1, x and y are the gray values of any two adjacent pixels, and N is the logarithm of (x_i, y_i). Image encryption mitigates the correlation between adjacent pixels by scrambling the pixel coordinates evenly. Employing this process in PV array reconfiguration is highly advantageous and suitable. In the TCT-configured array, all the parallel connected panels are connected in series to form a string (Figure 2D). So, if the panels of a particular row are shaded, the total string current is highly limited due to their series connection. Hence, using the concept of image encryption for reconfiguration relocate the panels in all rows thereby reducing the correlation between adjacent shaded panels in a particular row. This mitigates the mismatch and enhances the output. Hence, an efficient technique is required to mitigate the correlation between adjacent pixels. By employing the DS alone does not rearrange the pixels effectively. So, to achieve minimum correlation, a calligraphy-based scan is executed as detailed in the subsequent section.

4.3 | Pixel rearrangement with calligraphy-based DS

Calligraphy is a visual art associated with writing. It is the design and execution of lettering with distinct shapes of a pen, ink brush, or another writing instrument. In simple terms, it is the art of writing the symbols and characters of any language. Whatever the accessories, the value is on the attractiveness and beauty of the writing, together with the expressivity and essence of line. In general, calligraphy is broadly classified into three types: Arabic calligraphy, western calligraphy, and oriental calligraphy.[43] These three calligraphic styles further consist of various lettering styles or fonts. The two sample calligraphy styles namely Edwardian script ITC font and Bradley hand ITC font[44] are shown in Figure 4.

The original 6 × 8 matrix and the corresponding scanned pattern obtained by various alphabets is shown in Figure 5. In this paper, a letter "W" of Edwardian script ITC font style is considered for calligraphy scanning of elements in a matrix. The reason for choosing the alphabet "W" is due to its effectiveness in yielding the lowest correlation

FIGURE 4 (A) Edwardian Script ITC font style and (B) Bradley Hand ITC font style

11	12	13	14	15	16	17	18
21	22	23	24	25	26	27	28
31	32	33	34	35	36	37	38
41	42	43	44	45	46	47	48
51	52	53	54	55	56	57	58
61	62	63	64	65	66	67	68

Original 6×8 matrix

21	31	22	13	14	23	32	41
51	33	24	15	16	25	34	43
52	61	62	53	44	35	26	17
18	27	36	45	54	63	64	55
46	28	38	56	65	11	12	42
66	37	47	57	67	48	58	68

Obtained by alphabet 'D'

12	21	31	22	13	14	23	32
41	51	42	33	24	25	34	43
61	62	53	44	35	26	27	36
45	54	63	64	55	46	37	28
38	56	65	11	52	15	16	17
37	47	57	67	18	48	58	68

Obtained by alphabet 'H'

12	21	31	22	13	14	23	32
41	51	42	33	24	15	16	25
34	43	61	62	53	44	35	26
18	27	36	45	54	63	64	55
46	37	28	47	56	65	66	57
67	11	52	17	38	48	58	68

Obtained by alphabet 'M'

12	21	31	22	13	14	23	41
51	42	33	24	16	25	34	43
61	62	53	44	35	26	18	27
36	45	54	63	64	55	46	37
28	56	65	11	32	52	15	66
17	47	57	67	38	48	58	68

Obtained by alphabet 'N'

21	31	22	13	14	23	32	41
51	42	33	24	15	16	25	34
43	52	61	62	53	44	35	26
17	27	36	45	54	63	55	46
28	38	56	65	66	11	12	64
37	47	57	67	18	48	58	68

Obtained by alphabet 'R'

31	22	13	14	23	32	41	51
33	24	25	34	43	52	62	53
44	35	26	17	27	36	45	54
63	64	55	46	37	28	38	47
56	65	11	21	61	12	42	15
16	66	57	67	18	48	58	68

Obtained by alphabet 'W'

31	22	13	14	23	32	41	51
42	33	24	15	25	34	43	52
61	62	53	44	35	26	17	18
27	36	45	54	63	64	55	46
37	28	47	56	65	66	57	11
21	12	16	67	38	48	58	68

Obtained by alphabet 'X'

12	21	31	22	13	14	23	32
41	51	42	33	24	15	25	34
43	52	53	44	35	36	45	54
63	64	55	46	37	28	47	56
65	66	11	61	62	16	26	17
47	57	67	18	38	48	58	68

Obtained by alphabet 'Y'

12	21	31	22	13	14	23	32
41	51	42	33	24	25	34	43
52	53	44	35	26	36	45	54
63	64	11	61	62	15	55	65
16	46	56	66	17	27	37	47
57	67	18	28	38	48	58	68

Obtained by alphabet 'Z'

FIGURE 5 Original 6 × 8 matrix and the corresponding scanned pattern obtained by various alphabets

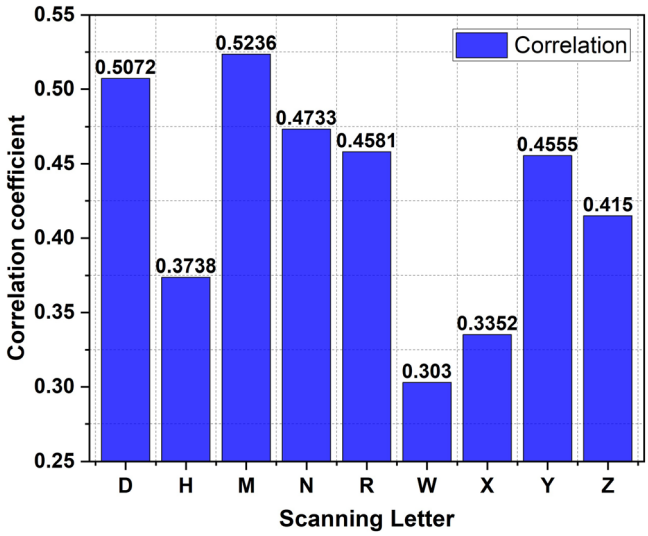

FIGURE 6 Correlation between adjacent pixels obtained by scanning with various alphabets

coefficient compared to other alphabets. The correlation coefficient (as mentioned in Section 4.2) obtained by scanning with some of the complex structured alphabets such as $\mathscr{D}, \mathscr{H}, \mathscr{M}, \mathscr{N}, \mathscr{R}, \mathscr{X}, \mathscr{W}, \mathscr{X}, \mathscr{Y}, \mathscr{Z}$ are given in Figure 6. It is noted from Figure 6 that the least correlation coefficient is obtained with "W" which is the most suitable alphabet for efficient rearrangement amongst all. Hence, the calligraphic letter "W" is coupled with the DS to efficiently rearrange the pixel coordinates. First, the proposed calligraphy-based DS is executed on the entire m × n matrix to rearrange its pixel coordinates which are visited by the considered English letter "W" of Edwardian Script ITC font. Second, the unvisited pixels coordinates are scanned column-wise and are arranged row-wise in a new rearranged matrix as shown in Figure 7A,B. The calligraphy-based DS with the letter "W" for an 8 × 8 and 8 × 6 matrices and the obtained rearranged pixel coordinates is shown in Figures 7 and 8, respectively.

Generally, in the image encryption proposes, the scan pattern starts from left to right as shown in Figure 3. However, a special case has also been experimented with where the DS starts from another corner of the matrix. If the DS starts from right to left, the correlation between adjacent pixels is found to be −0.2120, which is also very low. Hence, it

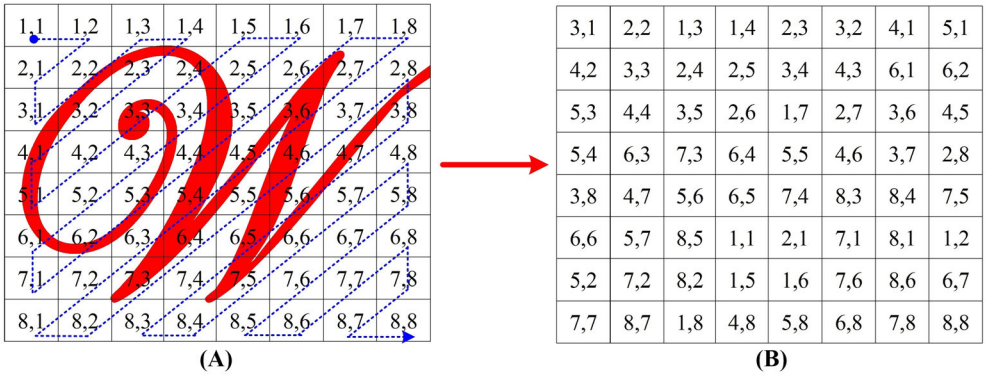

FIGURE 7 (A) Original matrix coordinates, (B) DS-based rearranged matrix coordinates of an 8 × 8 array

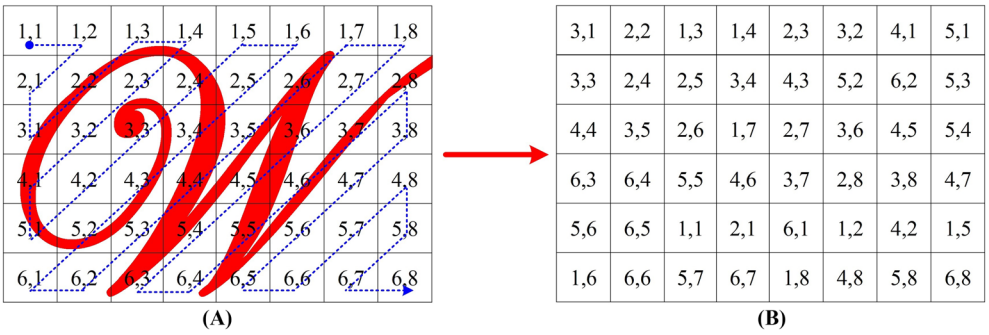

FIGURE 8 (A) Original matrix coordinates, (B) DS-based rearranged matrix coordinates of a 6 × 8 array

is noted that the least correlation is obtained by the proposed scanning pattern in both directions (left to right and vice versa) which results in superior performance.

4.4 | Calligraphy-based DS configuration of PV array

The proposed research work is based on the resemblance of a panel in the PV array with an individual pixel of an image. A popular DS integrated with a calligraphic approach is employed to obtain effective reconfiguration of PV panels without altering their electrical circuitry thereby mitigating the row current mismatch and enhancing the output power of the PV array under PS. In the proposed reconfiguration approach, the PV panels are physically relocated based on the obtained pattern of rearranged DS matrix while the electrical circuit remains the same. This does not provoke any variation in its electrical properties and consequently lessens the shading intensity by distributing the shade over the PV array. The development of the proposed DS reconfiguration approach is shown in Figure 9A–C. Figure 9A,B shows the unconnected panels of the TCT configuration and the DS arrangement of PV panels in an array. Figure 9C depicts the DS configured PV array without affecting the electrical circuit. Consequently, the proposed image processing-based PV array reconfiguration strategy results in maximum energy yield. The detailed flowchart of the proposed technique for reconfiguring the PV array is shown in Figure 10.

4.5 | Theoretical analysis and mathematical validation of the proposed configuration

To assess the approach of shade dispersion by DS-based array reconfiguration, a single-row shading case is considered for an 8 × 8 PV array as shown in TCT configuration of Figure 11. The current produced by an individual PV panel "I"

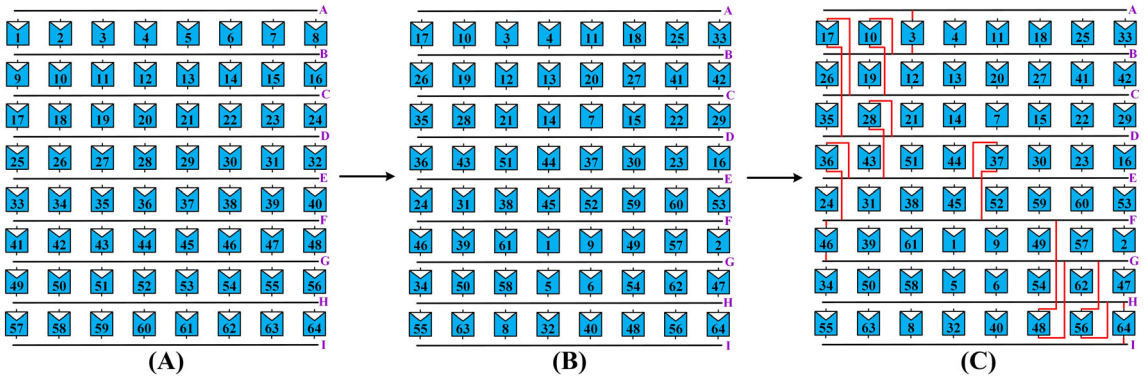

FIGURE 9 (A) Unconnected panels of TCT config., (B) DS arrangement of PV panels, (C) DS-configured PV array

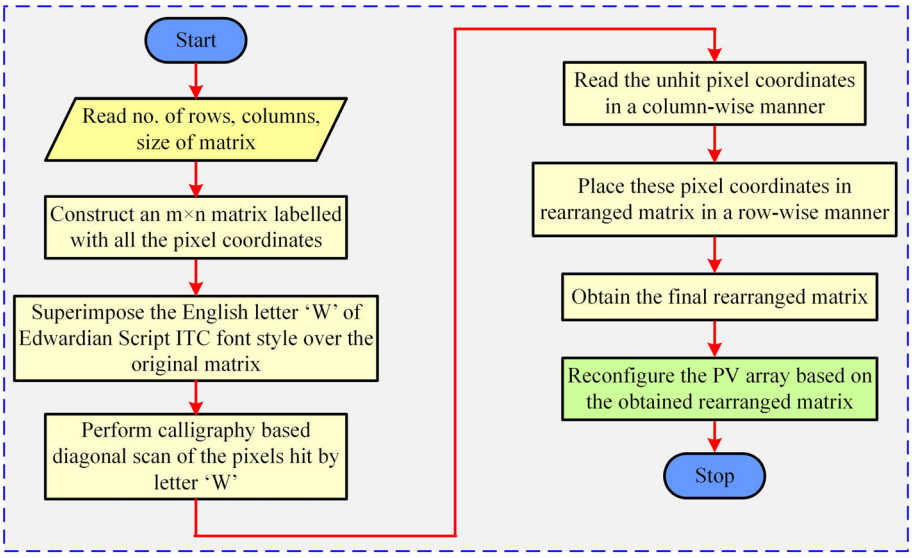

FIGURE 10 Flowchart of the calligraphy-based diagonal scan configuration of PV array

at a particular irradiation "Gi" is given as $I = (S.F) \times I_m$, and $S.F = Gi/G$, where S. F is the shading factor, and I_m denotes the current generated at STC of $G = 1000\ W/m^2$. Greater the incident solar irradiation on a panel higher is the current production. The array voltage "V_a" is the sum total of voltages of all the rows in an array which is given as

$$V_a = \sum_{i=1}^{a} V_{ij} \tag{7}$$

where V_{ij} is the voltage of the panels at jth row. By disregarding the voltage drop across bypass diodes, the voltage of an 8×8 PV array is $V_a = 8\ V_m$. According to KCL, the current across the individual node is obtained as

$$I_a = \sum_{j=1}^{b} \left(I_{ij} - I_{(i+1)j}\right) = 0, \quad \text{for } i = 1, 2, 3, \ldots\ldots\ldots, (i-1) \tag{8}$$

The output power "P_{PV}" obtained by an 8×8 PV array under normal conditions (without shading) is given as

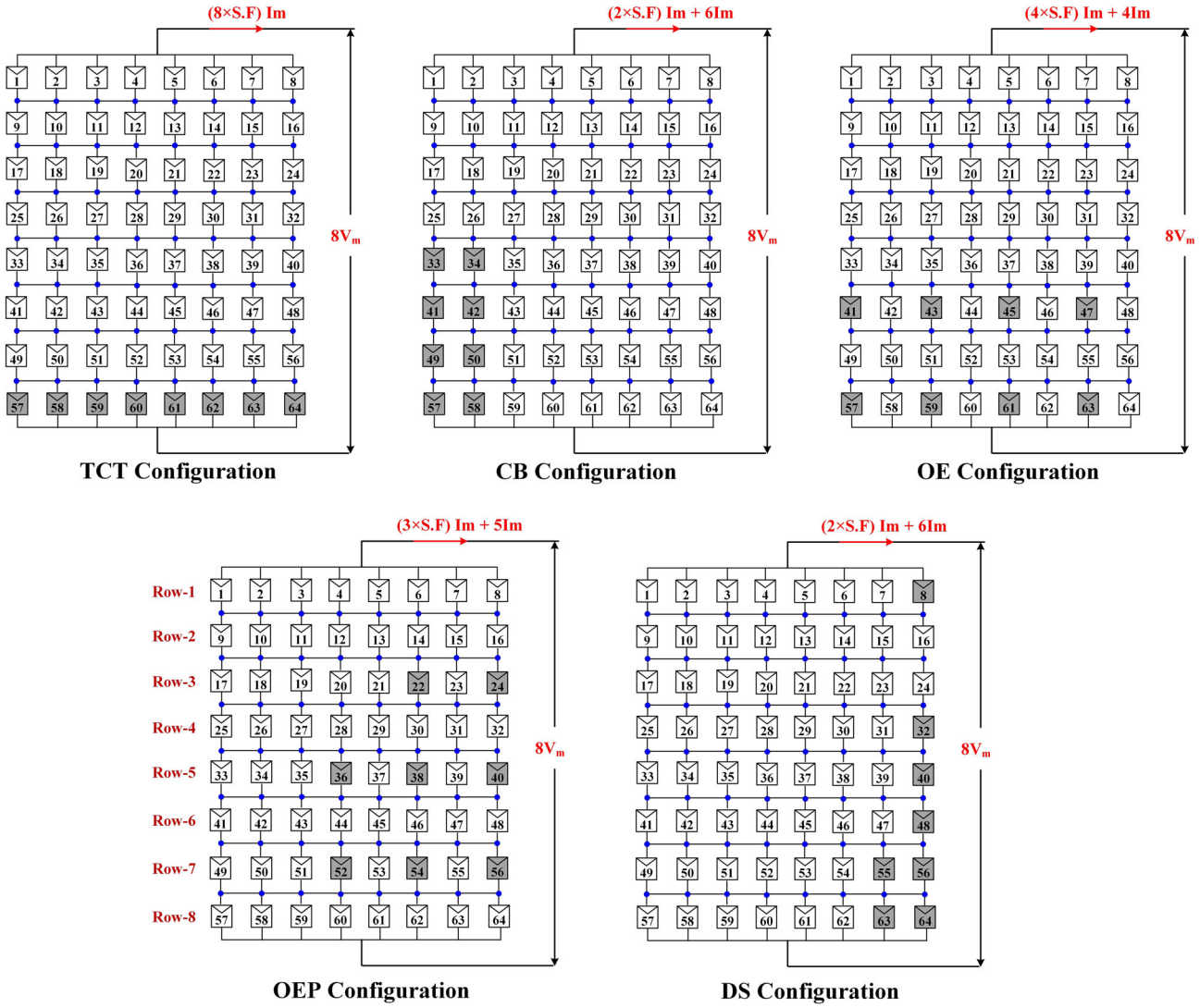

FIGURE 11 Shading on 8 × 8 PV array in TCT, CB,[26] OE,[34] OEP,[35] and DS configurations

$$P_a = V_a I_a = (8V_m)(8I_m) = 64V_m I_m \tag{9}$$

The shading in TCT configuration and the corresponding shade dispersal through CB,[26] OE,[34] OEP,[35] and proposed DS is illustrated in Figure 11.

4.5.1 | Power generation by conventional TCT configuration

The considered row-type shading condition on a TCT configured PV array is shown in Figure 11. All the panels in the last row of an 8 × 8 PV array are considered to be shaded receiving lower irradiation levels (S.F < 1) while the remaining portion of the array receives maximum irradiation. The PV panels in row-1 receive maximum irradiation and hence the current generated by them is given as

$$I_{R1} = \sum_{j=1}^{8} SF_{1j} I_m = SF_{11} I_m + SF_{12} I_m + SF_{13} I_m + SF_{14} I_m + SF_{15} I_m + SF_{16} I_m + SF_{17} I_m + SF_{18} I_m \tag{10}$$

where $SF_{11} = \frac{G_{11}}{G} = 1;\ SF_{12} = \frac{G_{12}}{G} = 1; SF_{13} = \frac{G_{13}}{G} = 1; \ldots\ldots SF_{18} = \frac{G_{18}}{G} = 1;$

$$I_{R1} = \sum_{j=1}^{8} SF_{1j} I_m = 8I_m$$

Similarly, the current generated by the panels in row-2 to row-7 is given as

$$I_{R2} = I_{R3} = I_{R4} = I_{R5} = I_{R6} = I_{R7} = 8I_m \tag{11}$$

The panels in row-8 are shaded hence receiving lower irradiation based on the shading factor. The current generated by row-8 of the PV array is given as

$$\begin{aligned} I_{R8} = \sum_{j=1}^{8} SF_{8j} I_m = SF_{81} I_m + SF_{82} I_m + SF_{83} I_m + SF_{84} I_m + SF_{85} I_m \\ + SF_{86} I_m + SF_{87} I_m + SF_{88} I_m \end{aligned} \tag{12}$$

and $SF_{81} = \frac{G_{81}}{G} = SF; SF_{82} = \frac{G_{82}}{G} = SF;\ SF_{83} = \frac{G_{83}}{G} = SF; \ldots\ldots SF_{88} = \frac{G_{88}}{G} = SF;$

where shading Factor, $SF < 1$

$$I_{R8} = (8 \times SF) I_m$$

The panels in the series–parallel PV array configuration are interconnected to form a Total-Cross-Tied PV configuration. Due to the series connection of rows in the TCT-configured array, the total array current is restricted to $(8 \times SF) I_m$. Accordingly, the power produced by conventional TCT is given as

$$P_{a,TCT} = V_a I_a = (8V_m)((8 \times SF) I_m) = (64 \times SF) V_m I_m, \text{ where SF} < 1 \tag{13}$$

4.5.2 | Power generation by CB configuration

The concentrated shade in the conventional TCT configuration is distributed over the PV Array by employing the reconfiguration strategy based on the CB approach as depicted in Figure 11. Due to the shade dispersal, the output power is enhanced by decreasing the mismatches between the rows of an array. The row currents of the first four rows (from row-1 to row-4) are given as follows:

$$I_{R1} = \sum_{j=1}^{8} SF_{1j} I_m = 8I_m \tag{14}$$

Similarly, the current generated by the panels in row-2 to row-4 is given as

$$I_{R2} = I_{R3} = I_{R4} = 8I_m \tag{15}$$

It is observed from Figure 11, that the eight shaded panels are distributed in last four rows. Thus, the current generated by row-5 to row-8 is given as

$$I_{R5} = I_{R6} = I_{R7} = I_{R8} = (2 \times SF) I_m + 6I_m \tag{16}$$

The current generated by CB is restricted to $(2 \times SF) I_m + 6I_m$, which is higher than conventional TCT due to its shade distribution. Consequently, the power produced by CB-based configuration is given as

$$P_{a,CBM} = V_a I_a = (8V_m)((2 \times SF)I_m + 6I_m) = ((16 \times SF) + 48)V_m I_m,\ SF < 1 \quad (17)$$

4.5.3 | Power generation by OE configuration

The shade dispersion of the concentrated shade by the existing OE configuration is shown in Figure 11. By OE, the shade is dispersed to row-6 and row-8 and, hence, their row currents are given by

$$I_{R6} = I_{R8} = (4 \times SF)I_m + 4I_m \quad (18)$$

However, the remaining rows receive maximum irradiation generating the currents as follows:

$$I_{R1} = I_{R2} = I_{R3} = I_{R4} = I_{R5} = I_{R7} = 8I_m \quad (19)$$

The total array current generated by OE configuration is limited to $(4 \times SF)I_m + 4I_m$, which is slightly higher than TCT. Thus, the power produced by OE-based configuration is given as:

$$P_{a,OE} = V_a I_a = (8V_m)((4 \times SF)I_m + 4I_m) = ((32 \times SF) + 32)V_m I_m,\ SF < 1 \quad (20)$$

4.5.4 | Power generation by OEP configuration

The OEP configuration offers slightly better performance compared to OE by dispersing the row-type shading to three rows (row-3, row-5, and row-7) as shown in Figure 11. The currents generated by row-3, is given by

$$I_{R3} = (2 \times SF)I_m + 6I_m \quad (21)$$

The corresponding row currents of row-5, and row-7 are given by

$$I_{R5} = I_{R7} = (3 \times SF)I_m + 5I_m \quad (22)$$

The remaining rows receive maximum irradiation generating the currents as follows:

$$I_{R1} = I_{R2} = I_{R4} = I_{R6} = I_{R8} = 8I_m \quad (23)$$

The array current generated by OEP configuration is restricted to $(3 \times SF)I_m + 5I_m$, which is slightly higher than TCT and OE. The array power produced by OEP-based configuration is

$$P_{a,OEP} = V_a I_a = (8V_m)((3 \times SF)I_m + 5I_m) = ((24 \times SF) + 40)V_m I_m,\ SF < 1 \quad (24)$$

4.5.5 | Power generation by DS configuration

The DS configuration of the PV array disseminates the concentrated row-type shade in conventional TCT to various rows as depicted in Figure 11. Due to its effective shade dispersal, the mismatch between the rows of an array is highly mitigated thereby maximizing the output power. The shade is now dispersed to row-1, row-4, row-5, row-6, row-7, and row-8, respectively. After DS-based reconfiguration, one shaded panel exists in row-1, row-4, row-5, and row-6 thereby generating the current as follows:

$$I_{R1} = I_{R4} = I_{R5} = I_{R6} = (1 \times SF)I_m + 7I_m \quad (25)$$

whereas there exist two shaded panels in row-7 and row-8 generating the current as follows:

$$I_{R7} = I_{R8} = (2 \times SF)I_m + 6I_m \tag{26}$$

Due to its effective shade dispersal, the current generated by DS configuration is limited to $(2 \times SF)I_m + 6I_m$ theoretically, which is relatively higher than all the conventional SP, TCT, and existing CB, OE, and OEP configurations. Therefore, the power delivered by DS-based configuration is given as

$$P_{a,DS} = V_a I_a = (8V_m)((2 \times SF)I_m + 6I_m) = ((16 \times SF) + 48)V_m I_m, \ SF < 1 \tag{27}$$

4.5.6 | Mismatch power

Due to the current restriction by series connected PV panels, the power produced by the shaded PV panels is always lower than the power produced by unshaded PV panels. Generally, the mismatch power (MMp) is given as

$$MM_P(W) = GMP_{STC} - GMP_{PS}$$

The mismatch power obtained by conventional TCT configuration is

$$MM_{P,TCT} = P_a - P_{a,TCT} = (64V_m I_m) - ((64 \times SF)V_m I_m) = 64(1 - SF)V_m I_m \tag{28}$$

The mismatch power obtained by existing CB configuration is

$$MM_{P,CB} = P_a - P_{a,CBM} = (64V_m I_m) - ((16 \times SF) + 48)V_m I_m = 16(1 - SF)V_m I_m \tag{29}$$

The mismatch power obtained by existing OE configuration is

$$MM_{P,OE} = P_a - P_{a,OE} = (64V_m I_m) - ((32 \times SF) + 32)V_m I_m = 32(1 - SF)V_m I_m \tag{30}$$

The mismatch power obtained by existing OEP configuration is

$$MM_{P,OEP} = P_a - P_{a,OEP} = (64V_m I_m) - ((24 \times SF) + 40)V_m I_m = 24(1 - SF)V_m I_m \tag{31}$$

The mismatch power obtained by proposed DS configuration is

$$MM_{P,DS} = P_a - P_{a,DS} = (64V_m I_m) - ((16 \times SF) + 48)V_m I_m = 16(1 - SF)V_m I_m \tag{32}$$

From the theoretical analysis, it has been noted that the performance of CB and DS is slightly on par with each other. But the proposed DS exhibit superior shade dispersion ability compared to CB as shown in Figure 11. Hence, in the practical scenario DS configuration exhibit comparatively superior performance. For instance, the considered shading case is simulated in MATLAB by assuming the irradiation of 900 and 400 W/m^2 incident on unshaded and shaded panels. From simulated results, it is noted that the CB and DS configurations yield the GMP of 10,416 and 10,533 W, respectively. From the Equations (28)–(32), it is evidently noted that $MM_{P,DS} < MM_{P,CB} < MM_{P,OEP} < MM_{P,OE} < MM_{P,TCT}$. Thus, by employing the DS-based configuration of PV panels, the mismatch power is highly mitigated thereby maximizing the output power irrespective of incident solar irradiation.

5 | PERFORMANCE INDICES

The following performance indices are considered to analyse the system under shading:

5.1 | Mismatch power (MM_P)

The mismatch power occurs due to the interconnection of solar PV cells with different characteristics,[45] and it is calculated by taking the difference between GMP obtained under STC, GMP_{STC} and GMP obtained under PS conditions, GMP_{PS}.

$$MM_P(W) = GMP_{STC} - GMP_{PS}$$

5.2 | Percentage power loss (P_L)

It is the ratio of the obtained mismatch power to the GMP obtained under STC.

$$P_L(\%) = \frac{GMP_{STC} - GMP_{PS}}{GMP_{STC}}$$

5.3 | Array yield (Y_A)

It gives the total number of hours necessitated by the PV array to generate the energy at its rated capacity.[46] It is the ratio of DC energy generated from the array ($E_{dc,\ array}$) to its rated capacity.

$$Y_A(h/day) = \frac{E_{dc,array}}{P_{rated}}$$

5.4 | Capacity factor (CF)

It is the ratio of the energy generated from PV system over a specific time (E_{actual}) to its rated capacity of the plant ($P_{pv,rated}$) generally calculated for a day/year.

$$CF = \frac{E_{actual}}{P_{PV,rated}}$$

5.5 | Fill factor (FF)

It is the ratio of the global maximum power to the product of open circuit voltage (V_{oc}) and short circuit current (I_{sc}). It is calculated as follows:

$$FF = \frac{V_{mpp} \times I_{mpp}}{V_{oc} \times I_{sc}}$$

5.6 | Efficiency (η)

It is the ratio of PV array output to the amount of incident solar irradiation (G in W/m^2) over the panel of area "A" (in mm^2) delivered by the sun. It is computed as follows:

$$\eta\,(\%) = \frac{V_{mpp} \times I_{mpp}}{G \times A}$$

5.7 | Performance ratio (PR)

It is obtained by taking the ratio of GMP obtained under PS conditions to the GMP obtained under STC. It gives what factor of the generated solar energy is utilized effectively.

$$PR(\%) = \frac{GMP_{PS}}{GMP_{STC}}$$

6 | RESULTS AND DISCUSSION

To mitigate the PS impacts, the PV array should be reconfigured in such a way that the shade is effectively dispersed over the entire array. The rows in an array experiencing maximum shadowing generate minimal current thereby limiting the overall PV array output. Hence, by effectively dispersing the shade through reconfiguring the PV array, the rows in an array that are generating less currents are significantly enhanced thereby reducing the row current variations between the rows and mismatch losses. For this purpose, a highly efficient calligraphy-based DS configuration is proposed.

6.1 | Analysis with even-symmetrical PV array

To determine the potency of the proposed DS technique over the other configurations, an 8 × 8 solar PV array with TCT, CB,[26] and DS configurations has been examined under six shading conditions employing MATLAB software. Further, the system is analyzed with the aforementioned eight performance indices. A 200-W Kyocera KG200GT PV panel is considered throughout the analysis. The GMP obtained by TCT configuration under unshaded conditions (STC) is 11,582 W. The shade dispersion with existing the CB technique is also shown for cases. The performance investigation of various configurations under six diverse PS conditions is conducted as follows:

6.1.1 | During case-1 shading

During this shading case, the first three rows of 8 × 8 PV array are considered to be shaded as shown in Figure 12A. The unshaded modules receive an irradiation of 900 W/m^2 and the shaded ones receive 600, 400, and 200 W/m^2. The shade dispersion with the proposed DS technique is shown in Figure 12C.

The comparison of row current computations of various configurations under case-1 shading is given in Table 1. From the table, it is noted that the conventional TCT configuration exhibit a broad row current variation ranging from 1.6Im to 7.2Im. However, the CB and DS configurations range from 3.8Im to 6.6Im and 4.2 m to 7.2Im respectively. The performance of CB and DS are on par with each other. Due to this significant reduction in the variation, the array characteristics of CB and DS are notably enhanced thus obtaining smoother curves as shown in Figure 13 respectively. The GMP obtained by TCT, CB, and DS configurations are 7122.8, 7536.3, and 7504.1 W, respectively. The output variation between CB and DS is less than 0.4%. The improved performance indices by employing the CB and proposed DS configurations are tabulated in Table 7.

6.1.2 | During case-2 shading

During case-2, one of the most prevalent shading patterns which is short and broad in nature is considered for the analysis as shown in Figure 14A. The shade dispersion with the proposed DS technique is shown in Figure 14C. In this

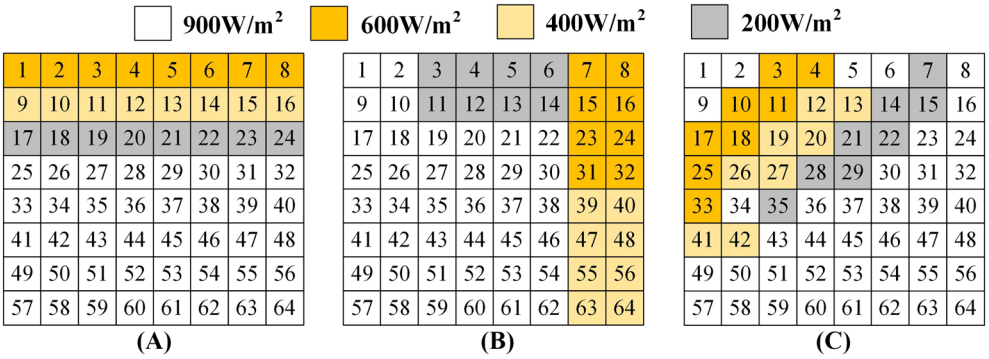

FIGURE 12 Case-1 shading pattern in (A) TCT, (B) CB, and (C) DS-based array configurations

TABLE 1 Comparison of row-current computations of TCT, CB, and DS configurations under Case-4 shading

TCT configuration	CB configuration[26]	DS configuration
$I_3 = (8 \times 0.2I_m) = 1.6I_m$ $I_2 = (8 \times 0.4I_m) = 3.2I_m$ $I_1 = (8 \times 0.6I_m) = 4.8I_m$ $I_4 = I_5 = I_6 = I_7 = I_8$ $= (8 \times 0.9I_m) = 7.2I_m$	$I_1 = I_2 = (4 \times 0.2I_m) + (2 \times 0.6I_m)$ $+ (2 \times 0.9I_m) = 3.8I_m$ $I_5 = I_6 = I_7 = I_8 = (6 \times 0.9I_m)$ $+ (2 \times 0.4I_m) = 6.2I_m$ $I_3 = I_4 = (6 \times 0.9I_m) + (2 \times 0.6I_m)$ $= 6.6I_m$	$I_2 = I_3 = (2 \times 0.9I_m) + (2 \times 0.6I_m) + (2 \times 0.4I_m)$ $+ (2 \times 0.2I_m) = 4.2I_m$ $I_4 = (3 \times 0.9I_m) + (1 \times 0.6I_m) + (2 \times 0.4I_m)$ $+ (2 \times 0.2I_m) = 4.5I_m$ $I_1 = (5 \times 0.9I_m) + (2 \times 0.6I_m) + (1 \times 0.2I_m) = 5.9I_m$ $I_5 = (6 \times 0.9I_m) + (1 \times 0.6I_m) + (1 \times 0.2I_m) = 6.2I_m$ $I_6 = (6 \times 0.9I_m) + (2 \times 0.4I_m) = 6.2I_m$ $I_7 = I_8 = (8 \times 0.9I_m) = 7.2I_m$

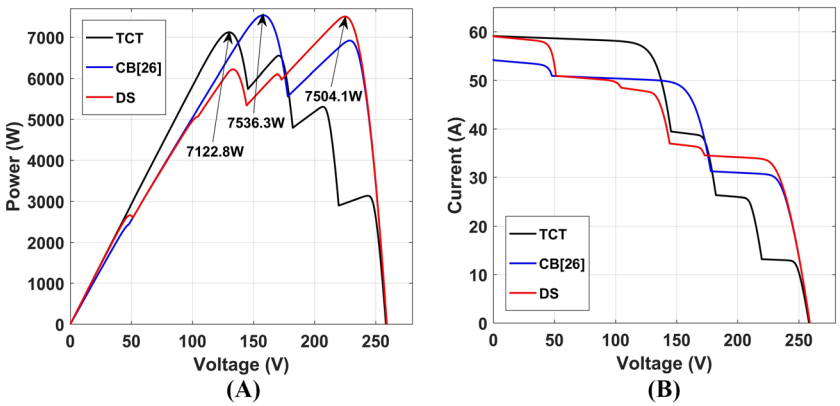

FIGURE 13 (A) PV and (B) IV characteristics of TCT, CB, and DS configurations under case-1 shading

shading condition, the shaded modules are regarded to receive irradiation of 500, 300, and 100 W/ m^2, whereas the unshaded modules receive 900 W/m^2.

The comparison of row-current computations of TCT, CB, and DS configurations under case-2 shading is given in Table 2. From the table, it is observed that the standard TCT configuration yields the largest row current variation which is in the range of 0.8Im to 7.2Im. This large variation is very significantly reduced by the proposed DS configuration which is in the range of 4.6Im to 6.4Im, thereby providing smooth array characteristics as shown in Figure 15. Followed by DS, CB configuration has the row currents ranging from 4.0Im to 7.2Im.

The GMP obtained by TCT, CB, and the proposed DS configurations is 7122.7, 7137.4, and 7980 W respectively. When compared to TCT and CB configurations, the proposed DS configuration enhances the GMP by 12.04% and 11.83%, respectively. By employing the proposed technique, the mismatch losses and percentage power loss are also

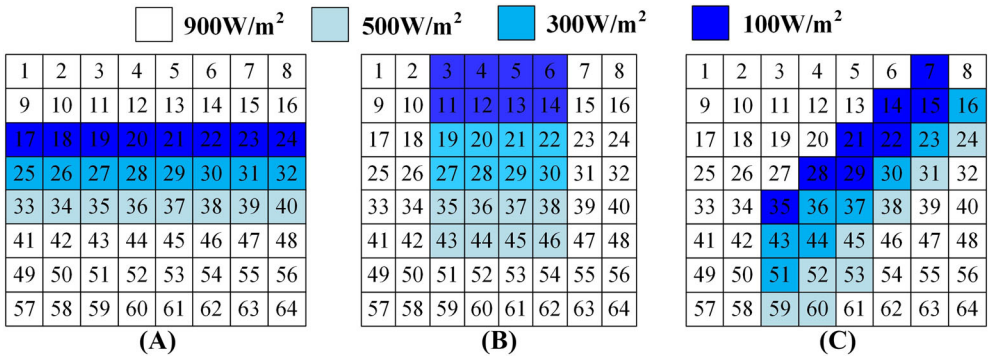

FIGURE 14 Case-2 shading pattern in (A) TCT, (B) CB, and (C) DS-based array configurations

TABLE 2 Comparison of row-current computations of TCT, CB, and DS configurations under case-2 shading

TCT configuration	CB configuration[26]	DS configuration
$I_3 = (8 \times 0.1I_m) = 0.8I_m$ $I_4 = (8 \times 0.3I_m) = 2.4I_m$ $I_5 = (8 \times 0.5I_m) = 4.0I_m$ $I_1 = I_2 = I_6 = I_7 = I_8$ $= (8 \times 0.9I_m) = 7.2I_m$	$I_1 = I_2 = (4 \times 0.9I_m) + (4 \times 0.1I_m)$ $= 4.0I_m$ $I_3 = I_4 = (4 \times 0.9I_m) + (4 \times 0.3I_m)$ $= 4.8I_m$ $I_5 = I_6 = (4 \times 0.9I_m) + (4 \times 0.5I_m)$ $= 5.6I_m$ $I_7 = I_8 = (8 \times 0.9I_m) = 7.2I_m$	$I_3 = I_4 = (4 \times 0.9I_m) + (2 \times 0.1I_m) + (1 \times 0.3I_m)$ $+ (1 \times 0.5I_m) = 4.6I_m$ $I_5 = (4 \times 0.9I_m) + (1 \times 0.1I_m) + (2 \times 0.3I_m)$ $+ (1 \times 0.5I_m) = 4.8I_m$ $I_2 = (5 \times 0.9I_m) + (2 \times 0.1I_m) + (1 \times 0.3I_m) = 5.0I_m$ $I_6 = (5 \times 0.9I_m) + (2 \times 0.3I_m) + (1 \times 0.5I_m) = 5.6I_m$ $I_7 = (5 \times 0.9I_m) + (2 \times 0.50I_m) + (1 \times 0.3I_m) = 5.8I_m$ $I_1 = (7 \times 0.9I_m) + (1 \times 0.1I_m) = 6.4I_m$ $I_8 = (6 \times 0.9I_m) + (2 \times 0.5I_m) = 6.4I_m$

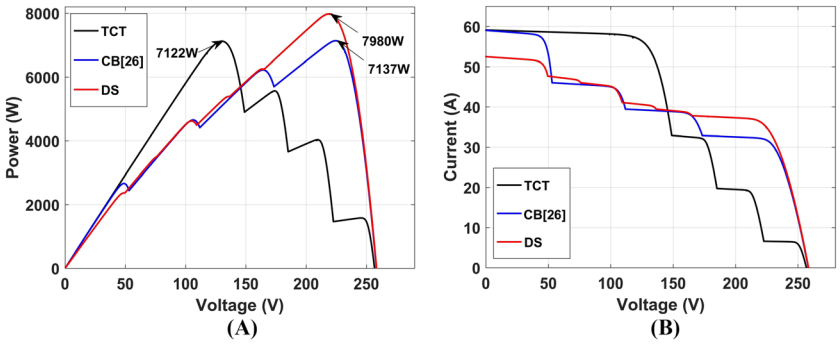

FIGURE 15 (A) PV and (B) IV characteristics of TCT, CB, and DS configurations under case-2 shading

greatly reduced to 3602 W, which is 31.09% less compared to both CB and TCT configurations. It is exceptionally substantiated in the fact that the values of Y_A (4.823 h/day), CF (0.201), FF (0.583), efficiency (13.1%), and PR (68.9%) of the proposed DS configuration are higher than the other configurations.

6.1.3 | During case-3 shading

During case-3, the shading pattern considered is short and narrow typed where the bottom right corner of the PV array is shaded as shown in Figure 16A and the shade dispersion with the proposed DS technique is shown in Figure 16C.

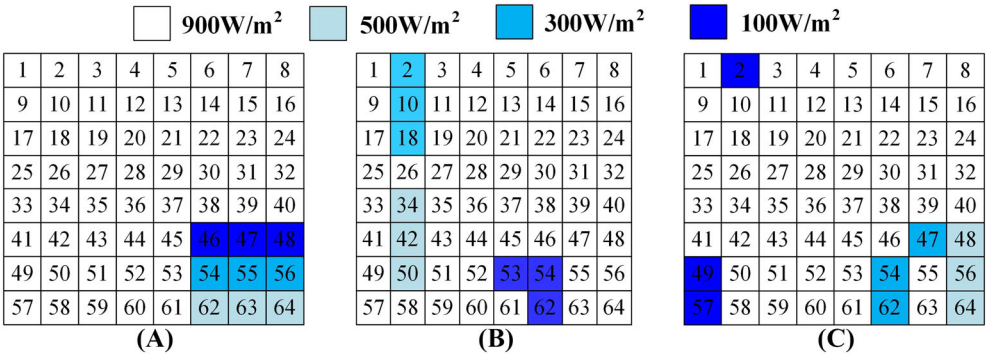

FIGURE 16 Case-3 shading pattern in (A) TCT, (B) CB, and (C) DS-based array configurations

TABLE 3 Comparison of row-current computations of TCT, CB, and DS configurations under case-2 shading

TCT configuration	CB configuration[26]	DS configuration
$I_6 = (5 \times 0.9I_m) + (3 \times 0.1I_m) = 4.8I_m$ $I_7 = (5 \times 0.9I_m) + (3 \times 0.3I_m) = 5.4I_m$ $I_8 = (5 \times 0.9I_m) + (3 \times 0.5I_m) = 6.0I_m$ $I_1 = I_2 = I_3 = I_4 = I_5 = (8 \times 0.9I_m) = 7.2I_m$	$I_7 = (5 \times 0.9I_m) + (1 \times 0.5I_m) + (2 \times 0.1I_m) = 5.2I_m$ $I_8 = (7 \times 0.9I_m) + (1 \times 0.1I_m) = 6.4I_m$ $I_1 = I_2 = I_3 = (7 \times 0.9I_m) + (1 \times 0.3I_m) = 6.6I_m$ $I_5 = I_6 = (7 \times 0.9I_m) + (1 \times 0.5I_m) = 6.8I_m$ $I_4 = (8 \times 0.9I_m) = 7.2I_m$	$I_7 = I_8 = (5 \times 0.9I_m) + (1 \times 0.1I_m) + (1 \times 0.3I_m) + (1 \times 0.5I_m) = 5.4I_m$ $I_6 = (6 \times 0.9I_m) + (1 \times 0.3I_m) + (1 \times 0.5I_m) = 6.2I_m$ $I_1 = (7 \times 0.9I_m) + (1 \times 0.1I_m) = 6.4I_m$ $I_2 = I_3 = I_4 = I_5 = (8 \times 0.9I_m) = 7.2I_m$

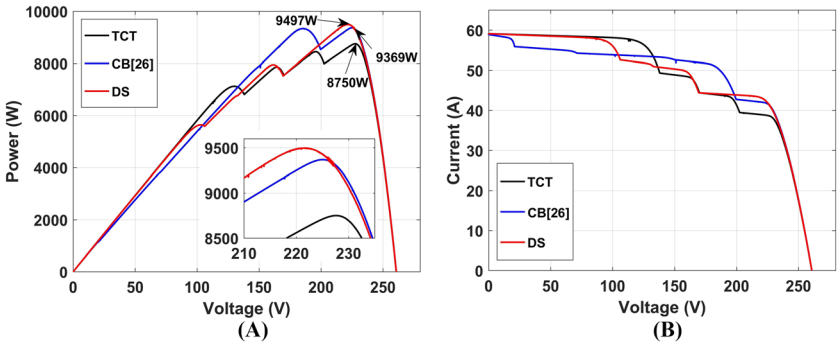

FIGURE 17 (A) PV and (B) IV characteristics of TCT, CB, and DS configurations under case-3 shading

From Table 3, it is noted that the proposed DS configuration improves the minimal row current from 4.8Im to 5.4Im and thus exhibiting the narrow row current variation, which is from 5.4Im to 7.2Im, whereas TCT and CB configurations exhibit comparatively a broad variation, which is from 4.8Im to 7.2Im and 5.2Im to 7.2Im respectively. The proposed DS configuration performs better than the existing CB in improving the minimal row current. From the PV characteristics shown in Figure 17A,B, it is observed that the DS configuration yields the highest GMP of 9497 W, which is 8.54% and 1.47% more than the TCT (8750.2 W) and CB (9369.1 W) configurations. The mismatch losses obtained by TCT and CB configurations are 2831.8 and 2212.9 W. The power losses obtained by TCT and CB configurations are 24.45% and 19.10%. The respective mismatch losses and power losses are further reduced to 2085 W and 18% by employing the proposed DS configuration.

6.1.4 | During case-4 shading

During this shading condition, the PV array experiences a shading that is long and broad shaped as shown in Figure 18A and the shade dispersion with DS technique is shown in Figure 18C. Table 4 gives the comparison of row-current computations of TCT, CB, and DS configurations under this shading condition. It is clearly evident from Table 4 that the standard TCT configuration exhibits a very large variation in the array row currents that range from 0.8Im to 7.2Im. The proposed DS configuration significantly enhances the least row current from 0.8Im to 3.8Im thereby mitigating the wide variation quite significantly to a narrow range of 3.8Im to 5.4Im. Due to this narrow variation, the proposed DS configuration renders very smooth array characteristics compared to both TCT and CB configurations as shown in Figure 19A,B, respectively.

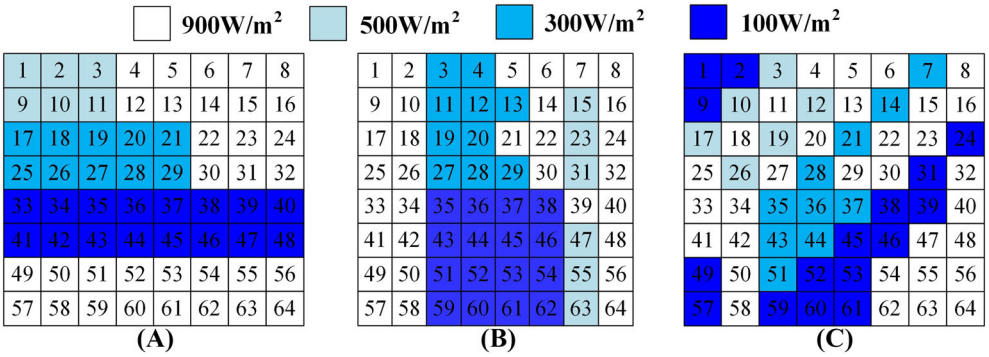

FIGURE 18 Case-4 shading pattern in (A) TCT, (B) CB, and (C) DS-based array configurations

TABLE 4 Comparison of row-current computations of TCT, CB, and DS configurations under case-4 shading

TCT configuration	CB configuration[26]	DS configuration
$I_5 = I_6 = (8 \times 0.1I_m) = 0.8I_m$ $I_3 = I_4 = (3 \times 0.9I_m) + (5 \times 0.3I_m) = 4.2I_m$ $I_1 = I_2 = (5 \times 0.9I_m) + (3 \times 0.5I_m) = 6.0I_m$ $I_7 = I_8 = (8 \times 0.9I_m) = 7.2I_m$	$I_6 = I_7 = I_8 = (3 \times 0.9I_m) + (4 \times 0.1I_m) + (1 \times 0.5I_m) = 3.6I_m$ $I_5 = (4 \times 0.9I_m) + (4 \times 0.1I_m) = 4.0I_m$ $I_2 = I_4 = (4 \times 0.9I_m) + (3 \times 0.3I_m) + (1 \times 0.5I_m) = 5.0I_m$ $I_1 = (6 \times 0.9I_m) + (2 \times 0.3I_m) = 6.0I_m$ $I_3 = (5 \times 0.9I_m) + (2 \times 0.3I_m) + (1 \times 0.5I_m) = 5.6I_m$	$I_5 = (3 \times 0.9I_m) + (3 \times 0.3I_m) + (2 \times 0.1I_m) = 3.8I_m$ $I_8 = (4 \times 0.9I_m) + (4 \times 0.1I_m) = 4.0I_m$ $I_7 = (4 \times 0.9I_m) + (1 \times 0.3I_m) + (3 \times 0.1I_m) = 4.2I_m$ $I_6 = (4 \times 0.9I_m) + (2 \times 0.3I_m) + (2 \times 0.1I_m) = 4.4I_m$ $I_1 = (4 \times 0.9I_m) + (2 \times 0.1I_m) + (1 \times 0.5I_m) + (1 \times 0.3I_m) = 4.6I_m$ $I_2 = I_3 = (4 \times 0.9I_m) + (2 \times 0.5I_m) + (1 \times 0.1I_m) + (1 \times 0.3I_m) = 5.0I_m$ $I_4 = (5 \times 0.9I_m) + (1 \times 0.5I_m) + (1 \times 0.3I_m) + (1 \times 0.1I_m) = 5.4I_m$

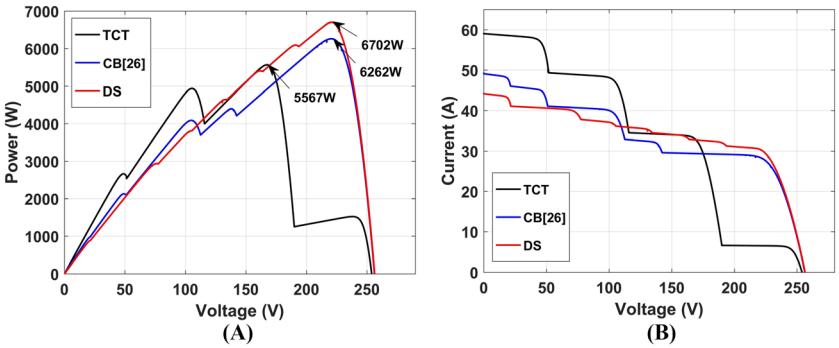

FIGURE 19 (A) PV and (B) IV characteristics of TCT, CB, and DS configurations under case-4 shading

The proposed DS configuration yields the highest GMP of 6702 W, which is 20.39% and 7.9% more compared to both standard TCT (5567.1 W) and CB (6262.5 W), respectively. Furthermore, DS configuration gives a peerless performance with a Y_A of 4.051 h/day, CF of 0.169, FF of 0.581, efficiency of 13.051%, and PR of 57.87%. Followed by DS, the CB configuration holds the subsequent place by proffering the Y_A of 3.785 h/day, CF of 0.158, FF of 0.488, efficiency of 12.19%, and PR of 54.07%. The TCT configuration gives a poor performance as the shade is not dispersed thereby rendering very unsatisfactory performance under this shading condition.

6.1.5 | During case-5 shading

During this shading condition, a part of a PV array is considered to be shadowed in a rectangular pattern as shown in Figure 20A. The shaded and unshaded modules receive an irradiation of 400 and 900 W/m^2. The comparison of row-current computations of TCT, CB, and DS configurations under the case-5 shading is given in Table 5.

From Table 5, it is evident that the proposed DS configuration not only enhances the least row current from 4.7Im to 5.7Im but also reduces the row current variation which ranges from 5.7Im to 6.7Im thus delivering smoother array characteristics as shown in Figure 21. When compared to DS, the TCT and CB configurations yield a broad range of row currents varying from 4.7Im to 7.2Im and 5.7Im to 7.2Im, respectively, and thus contains multiple power peaks in the characteristics. Further, the proposed DS configurations enhances the GMP by 1480.1 and 122.9 W, which is 17.81% and 1.49% more when compared to TCT and CB configurations respectively. Besides, the proposed DS configuration performed better than TCT and CB in giving an exceptional performance with the respective GMP, mismatch power, power loss, Y_A, CF, FF, efficiency, and PR values of 9793.1 W, 1788.9 W, 15.45%, 5.919/day, 0.247, 0.684, 13.86%, and 84.56%.

6.1.6 | During case-6 shading

During this case, the bottom part of the PV array is shaded as shown in Figure 22A and the respective shade dispersion with DS technique is shown in Figure 22C.

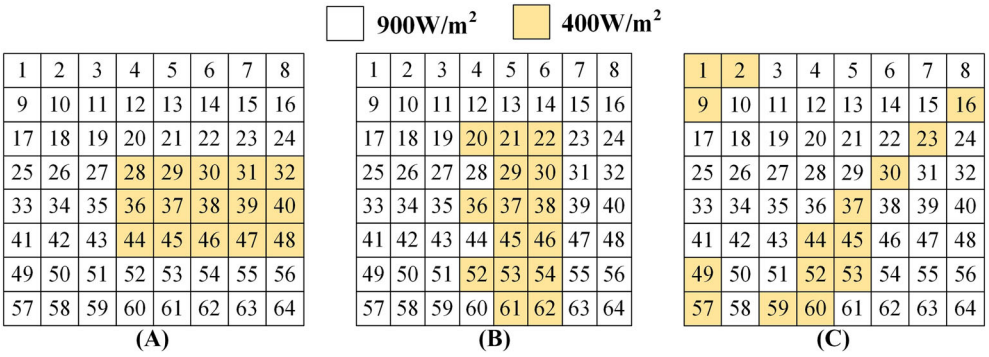

FIGURE 20 Case-5 shading pattern in (A) TCT, (B) CB, and (C) DS-based array configurations

TABLE 5 Comparison of row-current computations of TCT, CB, and DS configurations under Case-5 shading

TCT configuration	CB configuration[26]	DS configuration
$I_4 = I_5 = I_6 = (3 \times 0.9I_m) + (5 \times 0.4I_m) = 4.7I_m$ $I_1 = I_2 = I_3 = I_7 = I_8 = (8 \times 0.9I_m) = 7.2I_m$	$I_3 = I_5 = I_7 = (5 \times 0.9I_m) + (3 \times 0.4I_m) = 5.7I_m$ $I_4 = I_6 = I_8 = (6 \times 0.9I_m) + (2 \times 0.4I_m) = 6.2I_m$ $I_1 = I_2 = (8 \times 0.9I_m) = 7.2I_m$	$I_7 = I_8 = (5 \times 0.9I_m) + (3 \times 0.4I_m) = 5.7I_m$ $I_1 = I_2 = I_6 = (6 \times 0.9I_m) + (2 \times 0.4I_m) = 6.2I_m$ $I_3 = I_4 = I_5 = (7 \times 0.9I_m) + (1 \times 0.4I_m) = 6.7I_m$

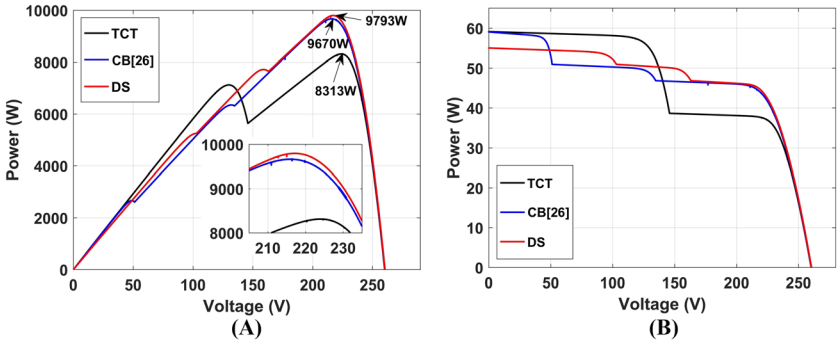

FIGURE 21 (A) PV and (B) IV characteristics of TCT, CB, and DS configurations under case-5 shading

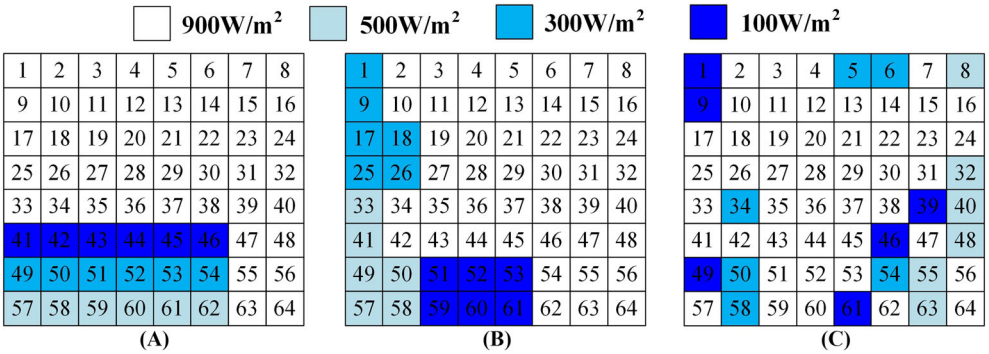

FIGURE 22 Case-6 shading pattern in (A) TCT, (B) CB, and (C) DS-based array configurations

TABLE 6 Comparison of row-current computations of TCT, CB, and DS configurations under case-6 shading

TCT configuration	CB configuration[26]	DS configuration
$I_6 = (6 \times 0.1I_m) + (2 \times 0.9I_m) = 2.4I_m$ $I_7 = (6 \times 0.3I_m) + (2 \times 0.9I_m) = 3.6I_m$ $I_8 = (6 \times 0.5I_m) + (2 \times 0.9I_m) = 4.8I_m$ $I_1 = I_2 = I_3 = I_4 = I_5 = (8 \times 0.9I_m) = 7.2I_m$	$I_7 = I_8 = (3 \times 0.9I_m) + (2 \times 0.5I_m) + (3 \times 0.1I_m) = 4.0I_m$ $I_3 = I_4 = (6 \times 0.9I_m) + (2 \times 0.3I_m) = 6.0I_m$ $I_1 = I_2 = (7 \times 0.9I_m) + (1 \times 0.3I_m) = 6.6I_m$ $I_5 = I_6 = (7 \times 0.9I_m) + (1 \times 0.5I_m) = 6.8I_m$	$I_1 = I_7 = (4 \times 0.9I_m) + (1 \times 0.1I_m) + (2 \times 0.3I_m) + (1 \times 0.5I_m) = 4.8I_m$ $I_5 = I_8 = (5 \times 0.9I_m) + (1 \times 0.5I_m) + (1 \times 0.3I_m) + (1 \times 0.1I_m) = 5.4I_m$ $I_6 = (6 \times 0.9I_m) + (1 \times 0.5I_m) + (1 \times 0.1I_m) = 6.0I_m$ $I_2 = (7 \times 0.9I_m) + (1 \times 0.1I_m) = 6.4I_m$ $I_3 = (8 \times 0.9I_m) = 7.2I_m$ $I_4 = (7 \times 0.9I_m) + (1 \times 0.5I_m) = 6.8I_m$

It is noted from Table 6 that the lowest variation in row current mismatch is obtained by the proposed DS which ranges from 4.8Im to 6.8Im, whereas the existing TCT and CB range from 2.4Im to 7.2Im and 4.0Im to 6.8Im respectively. The DS configuration yields the highest GMP of 8259.9 W, whereas the TCT and CB generate 6452.0 and 7223.7 W, respectively, as shown in Figure 23. Due to the effective shade dispersion by DS, the mismatch power is also significantly reduced. It is clearly evident from Figures 12C, 14C, 16C, 18C, 20C, and 22C that the proposed DS technique effectively disperses the shade over the entire array, whereas the existing CB technique disperses only in some part of array thus yielding reduced output compared to proposed technique. A comparative analysis of the eight aforementioned performance indices for TCT, CB, and DS configurations under six distinct shading conditions is shown in Table 7. Under all cases, the proposed DS exhibits the superior performance with enhanced values of GMP, FF, CF, Y_A, PR, and reduced MM_P. A comparative analysis of percentage enhancement in GMP by CB and DS configurations under case-1 to case-6 shading is shown in Figure 24.

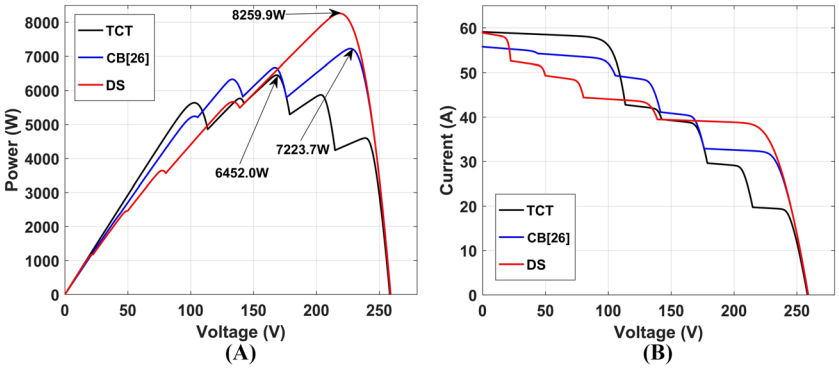

FIGURE 23 (A) PV and (B) IV characteristics of TCT, CB, and DS configurations under case-6 shading

TABLE 7 Comparative performance analysis of 8 × 8 PV array under case-1 to case-6 shading

Shading case	Config.	GMP (W)	MM_P (W)	P_L (%)	FF	η (%)	CF	Y_A (h/day)	PR (%)
Case-1	TCT	7122.8	4459.2	38.50	0.462	11.072	0.179	4.305	61.50
	CB[26]	7536.3	4045.7	34.93	0.534	11.715	0.19	4.555	65.07
	DS	7504.1	4077.9	35.21	0.487	11.665	0.189	4.535	64.79
Case-2	TCT	7122.7	4459.3	38.50	0.463	11.687	0.179	4.305	61.50
	CB[26]	7137.4	4444.6	38.38	0.463	11.711	0.18	4.314	61.62
	DS	7980.0	3602.0	31.10	0.583	13.094	0.201	4.823	68.90
Case-3	TCT	8750.2	2831.8	24.45	0.568	10.75	0.22	5.288	75.55
	CB[26]	9369.1	2212.9	19.11	0.608	11.51	0.236	5.663	80.89
	DS	9497.0	2085.0	18.00	0.617	11.667	0.239	5.74	82.00
Case-4	TCT	5567.1	6014.9	51.93	0.362	10.841	0.14	3.365	48.07
	CB[26]	6262.5	5319.5	45.93	0.488	12.195	0.158	3.785	54.07
	DS	6702.0	4880.0	42.13	0.581	13.051	0.169	4.051	57.87
Case-5	TCT	8313.0	3269.0	28.22	0.540	11.762	0.209	5.024	71.78
	CB[26]	9670.2	1911.8	16.51	0.628	13.682	0.244	5.845	83.49
	DS	9793.1	1788.9	15.45	0.683	13.856	0.247	5.919	84.55
Case-6	TCT	6452.0	5130.0	44.29	0.419	9.772	0.162	3.899	55.71
	CB[26]	7223.7	4358.3	37.63	0.497	10.941	0.182	4.366	62.37
	DS	8259.9	3322.1	28.68	0.536	12.511	0.208	4.992	71.32

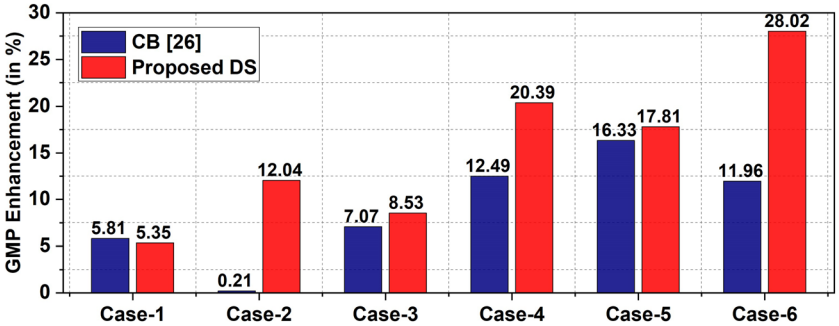

FIGURE 24 Percentage enhancement in GMP by CB and DS techniques under case-1 to case-6

6.1.7 | Extended analysis of proposed technique for 8 × 8 PV array

To further analyse the effectiveness of the proposed DS, 10 more distinct uniform shading patterns as shown in Figure 25 are considered for analysis. The shading case-7 to case-10 represents the shade due to the movement of clouds over the array and the other cases represent the static shade due to nearby towers, buildings, long poles, and trees, etc. It is noted from Figure 25 that the proposed DS exhibits effective shade dispersion thereby mitigating the mismatch losses. The GMP obtained by TCT and proposed DS configurations under case-7 to case-16 is shown in Figure 26. During all the shading cases, the proposed DS yields the highest GMP. By employing DS technique, the GMP is enhanced by 3.7%, 5.79%, 11.39%, 7.33%, 8.76%, 11.53%, 0.30%, 13.8%, 7.59%, and 9.8% under case-7 to case-16, respectively.

6.2 | Analysis with odd-symmetrical PV arrays

The proposed DS technique proved its effectiveness for an even-symmetric array as detailed in Section 6.1. In order to verify its effectiveness for odd-symmetric arrays, a 9 × 9 PV array is considered and tested under the very same shading patterns (shown in Sections 6.1.1 to 6.1.6) that have been considered for the 8 × 8 PV array.

The performance of the proposed DS technique is compared with the existing OE and OEP techniques under distinct shading conditions (as shown in Figure 27). The obtained PV characteristics under these shading cases are shown in Figure 28. It is noted from the figure, that the proposed DS exhibits superior and consistent performance yielding the highest GMP. On the contrary, the existing OE and OEP techniques exhibit highly inconsistent performance as shown in Figure 28. Hence, the proposed DS technique is proved to be effective for both even-symmetric and odd-symmetric PV arrays.

6.3 | Application of proposed technique to unsymmetrical PV arrays

A majority of the static reconfiguration techniques[14–26,28–33] reported in the literature are not compatible with unsymmetrical sizing of PV arrays such as 3 × 4, 5 × 9, and 13 × 8. In a practical scenario, the PV arrays can be symmetrical or asymmetric. Hence, their application is very narrow. Also, the major drawback of the existing CB technique is that it cannot be compatible with unsymmetrical PV arrays. To resolve this, very recently, two approaches based on Odd-Even (OE)[34] and Odd-Even-Prime (OEP)[35] patterned techniques are introduced. Nevertheless, both the OE and OEP techniques despite being scalable to any array sizes, exhibit very poor shade dispersion due to their ineffective reconfiguration. To validate the compatibility of the proposed DS for unsymmetrical PV arrays, an 8 × 6 PV array is considered. Further, to confirm the effectiveness of DS configuration, its performance has been compared with the existing OE and OEP-based array configurations. The various shading cases and their respective shade dispersion by OE, OEP, and DS techniques are shown in Figure 29.

It is observed from the figure that the proposed DS disperses the shade effectively over the entire array compared to OE and OEP techniques. It is evident from the array PV characteristics (shown in Figure 30 and Table 8), that the highest GMP is obtained by DS configuration. Moreover, the DS configuration exhibits comparatively better array characteristics that are close to the ideal characteristics.

6.3.1 | Effect of temperature variations on proposed configuration

In a practical scenario, the variation in solar irradiation affects the operating temperature of the PV cells. So, in this section, the temperature variation is also included in simulation studies to study the impact of temperature variation. The variation in temperature affects the array output voltage. For analysis, diverse temperature levels such as 25°C, 30°C, and 35°C are considered for demonstrating the impact on GMP obtained in TCT, OE, OEP, and DS-configured 8 × 6 PV array arrangements during shading case-23 and case-24. The corresponding array PV characteristics of an 8 × 6 PV array for 30°C and 35°C temperatures under are plotted as shown in Figures 31 and 32.

It is noted from the PV characteristics (in Figures 31 and 32) that the highest GMP is obtained by the proposed DS irrespective of variation in temperature. A comparative analysis of TCT, OE, OEP, and DS configurations of an 8 × 6 PV array under case-23 and case-24 for distinct temperatures is shown in Table 9.

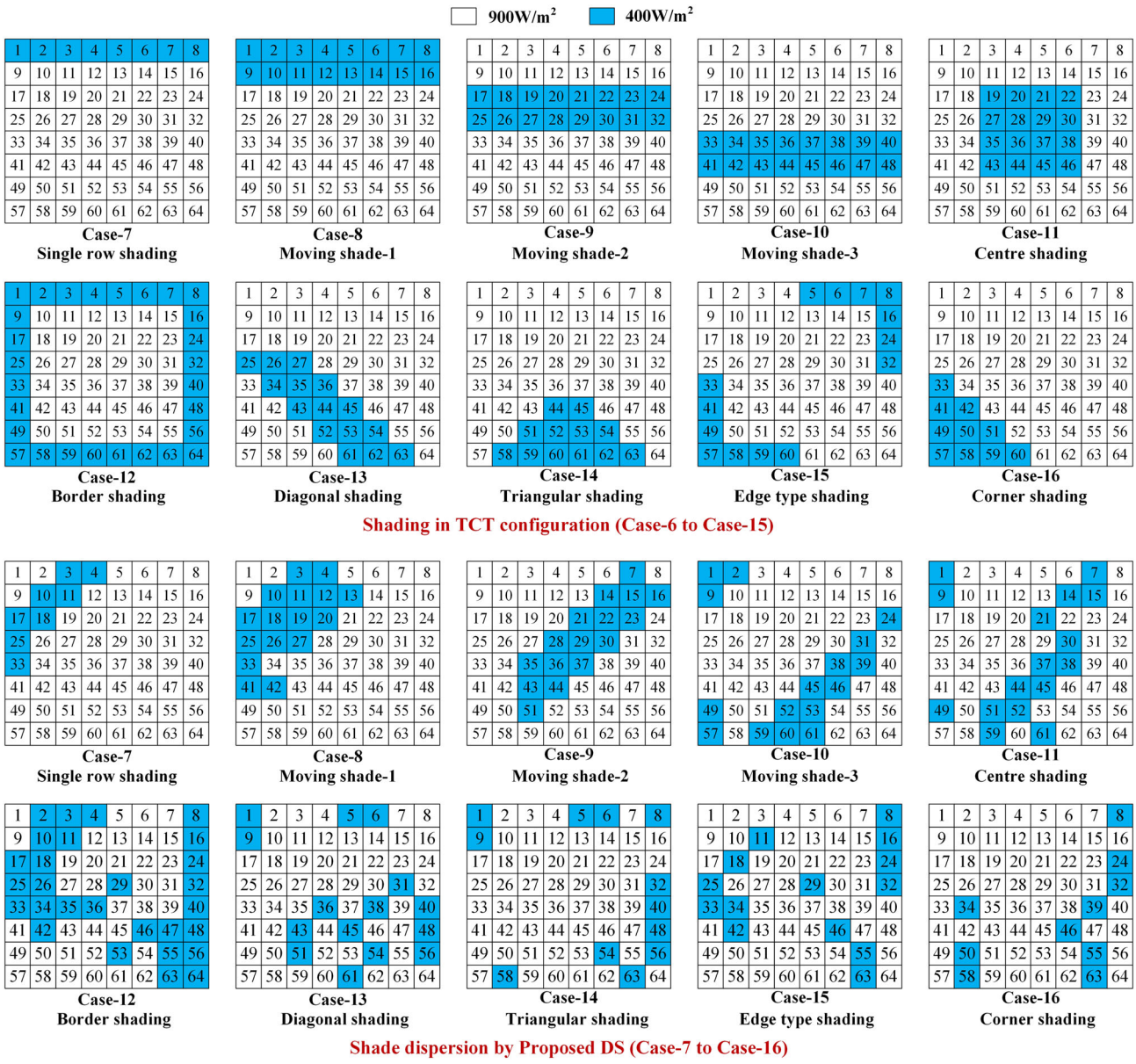

FIGURE 25 Additional shading cases (7–16): Shade in TCT and corresponding shade dispersion by DS

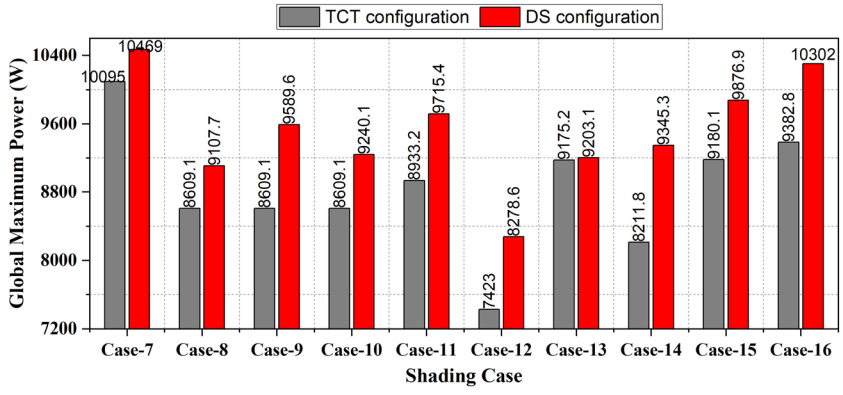

FIGURE 26 GMP (in watt) obtained under case-7 to case-16

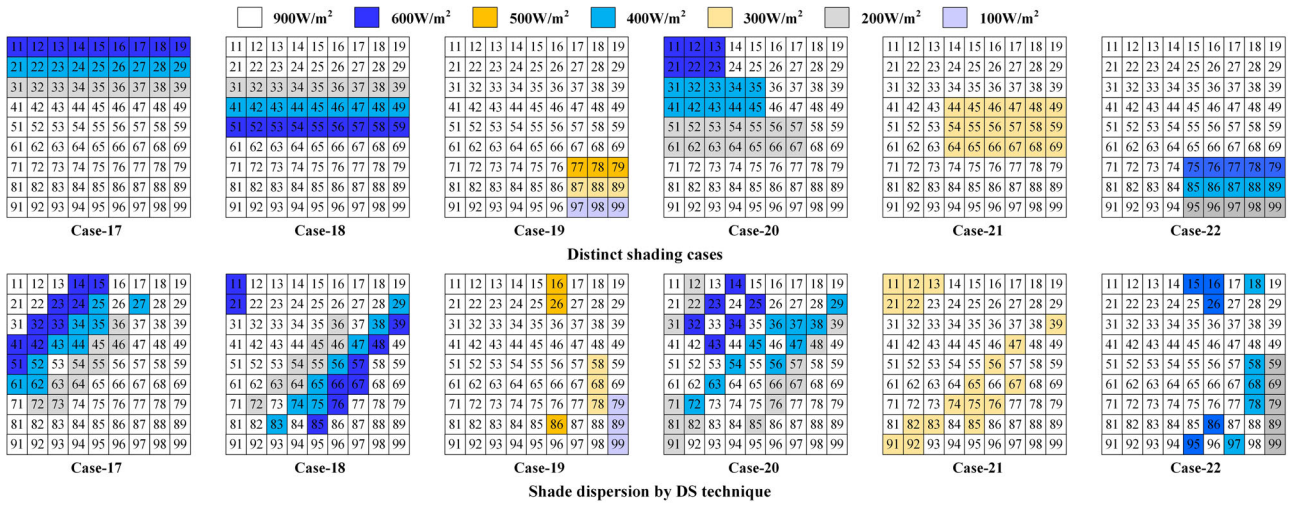

FIGURE 27 Distinct shading cases and their corresponding dispersion by DS

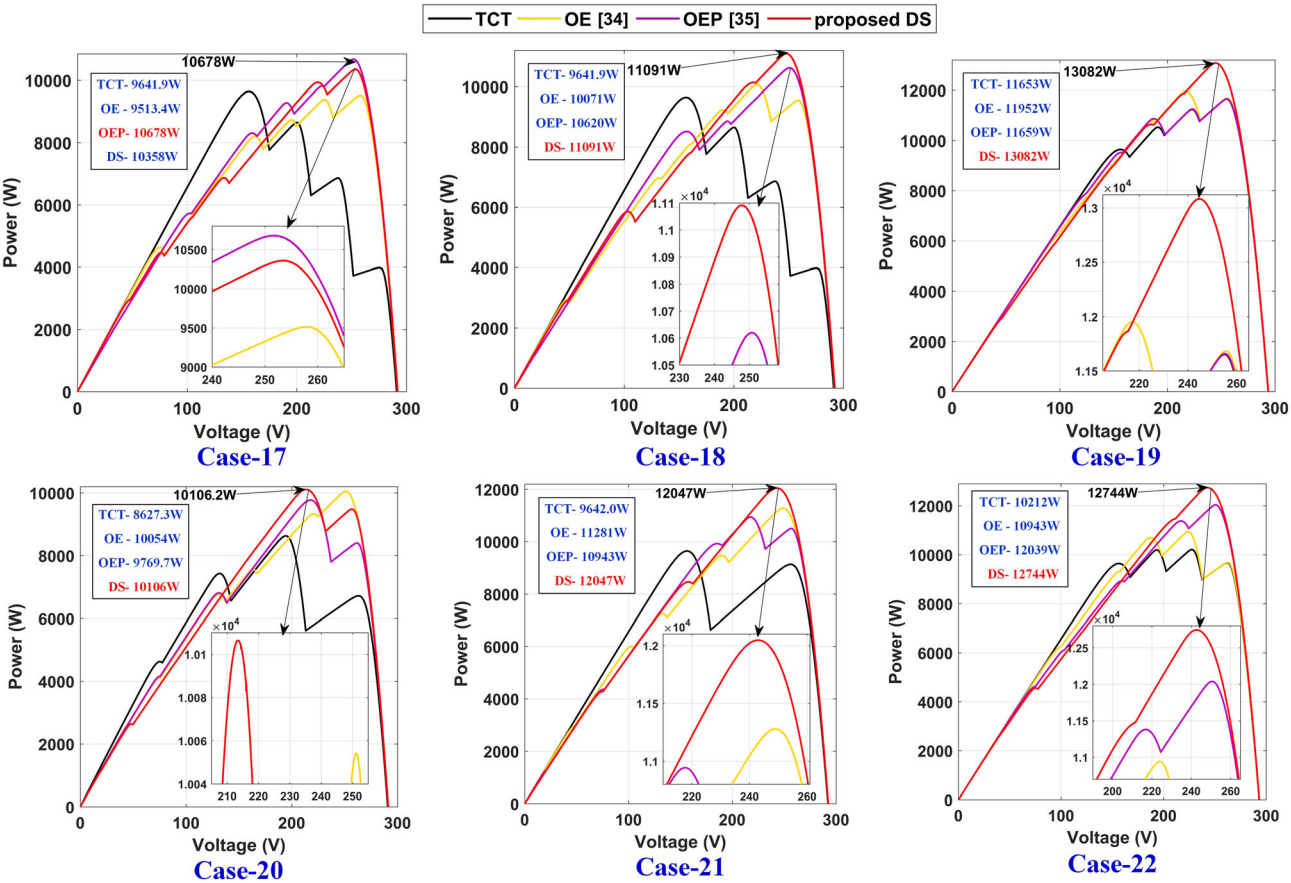

FIGURE 28 PV characteristics under shading case-17 to case-22

6.4 | Experimental validation of proposed configuration

To justify the theoretical and the obtained simulation results for TCT and DS configurations under shading conditions, a laboratory experimental setup is developed as shown in Figure 33. For experimentation purposes, 16 polycrystalline solar panels of each having 3-W capacity are connected in a 4 × 4 PV array of TCT and DS-based configurations

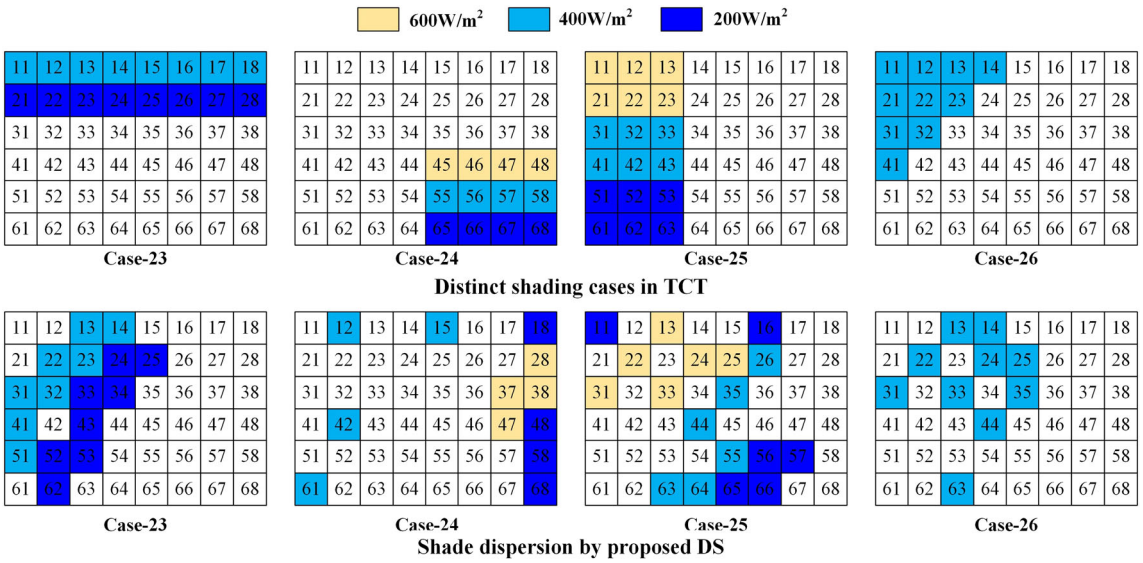

FIGURE 29 Shading cases 23 to 26 and corresponding shade dispersion

employing interconnection wires and banana plug connectors as shown in Figure 33. The output terminals of the 4 × 4 solar PV array are connected to a 300 Ω and 1.5 Ampere variable sliding rheostat. The rheostat is adjusted to set at a fixed point for extracting maximum power from the PV array. Two scientific digital multimeters are employed to measure the array voltage and the current flowing through the rheostat.

One portable solar power meter is used to measure the irradiation levels (in W/m^2) produced by the artificial light source. A digital infrared thermometer gun is used to measure the operating temperature of the PV panels. The solar panels receive the irradiation of 310 W/m^2 approximately by each lighting source under normal conditions. The shaded panels receive irradiation of about 160 W/m^2 and the temperature of the panels is measured to be 33°C. The PV panels are connected in both conventional benchmark TCT and the proposed DS configurations and tested under distinct shading cases as shown in Figure 34. The first three shading cases (case-27 to case-29) represent the shade of a moving cloud over the PV array with respect to time and the remaining cases (case-30 to case-34) represents the static shading (caused due to nearby buildings, long towers, poles, etc.) that remain for longer duration. The experimentation could have been conducted in the outdoor environment, however, the uncertainty and varying levels of the sun's irradiation, temperature, and other environmental factors affecting the output of the PV array yield misleading results while comparing the effectiveness of various configurations. Hence, the test is conducted in a laboratory setup where the configurations are tested under the same operating conditions.

It is clearly noted from Table 10 that the proposed DS configuration yield the highest outputs due to its effective shade dispersion under all the shading cases. The experimental hardware results are justified by comparing them with the obtained simulation results as shown in Table 10 and Figure 35. Hence, the efficacy and practical feasibility of the proposed DS are proved thereby functioning as an efficient solution in solving the shading-related issues.

6.5 | Qualitative comparison of various aspects of proposed DS with existing ones

- The existing conventional SP and TCT configurations have no shade dispersion capability thus leading to a greater mismatch in the row currents of an array. Further, the obtained array characteristics are also highly distorted from the ideal characteristics.
- Unlike the dynamic reconfiguration techniques,[5,6,8,9,12] the proposed DS configuration does not necessitate switches, sensors, switching matrix, switching controllers, relays, data acquisition systems, driver circuits, and complex algorithms for reconfiguration. The arrangement of PV panels based on the DS pattern can be established during the installation of the PV array itself.

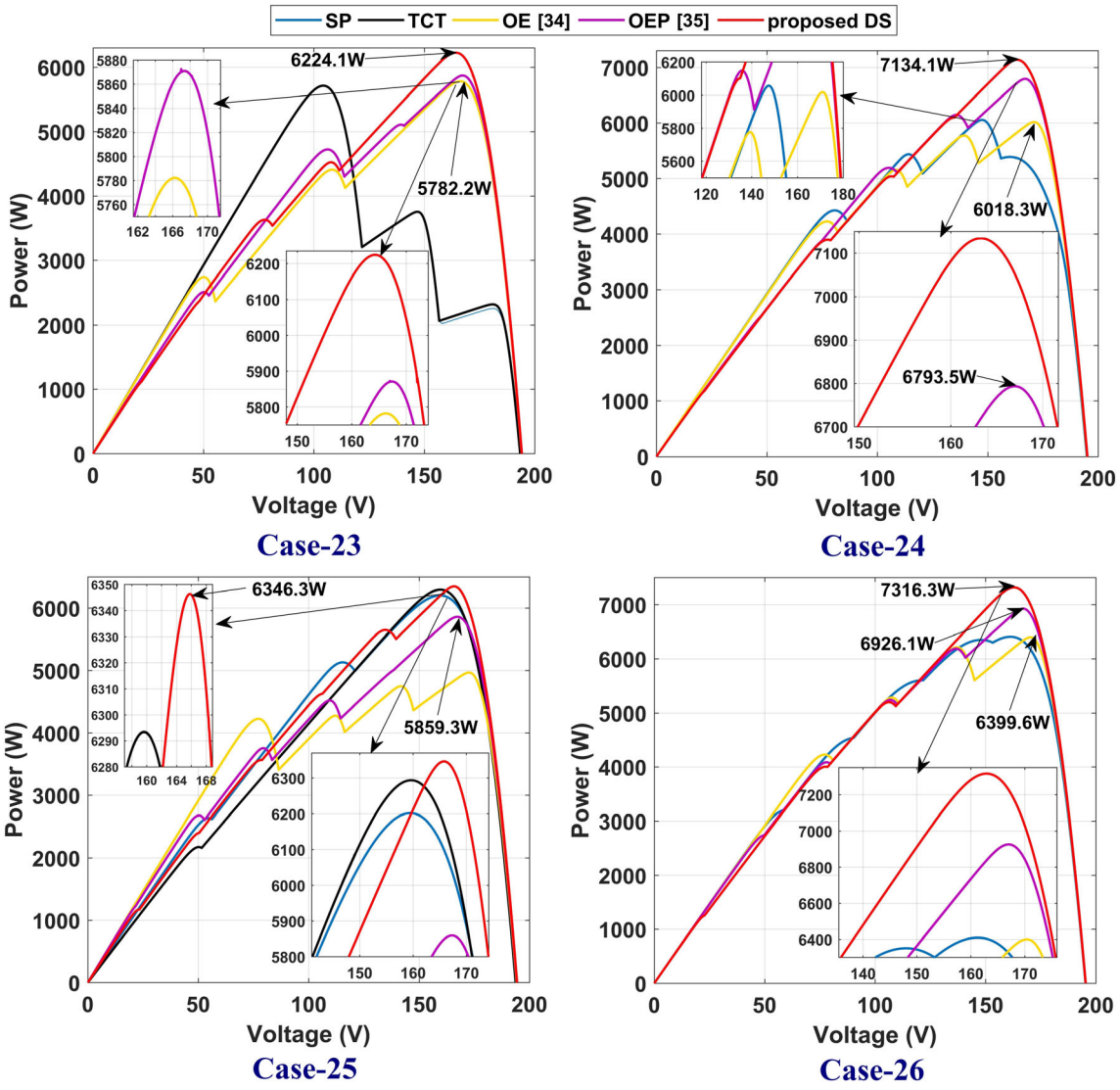

FIGURE 30 PV characteristics of 6 × 8 PV array for 25°C temperature under case-23 to 26

TABLE 8 GMP (in watt) of various configurations of a 6 × 8 array under case-23 to case-26

	Shading case							
	Case-23		Case-24		Case-25		Case-26	
Array config.	GMP	(% gain)	GMP	(% gain)	GMP	(% gain)	GMP	(% gain)
SP	5713.6	-	6056.6	0.72	6201.6	−1.46	6409.1	−7.49
TCT	5713.6	-	6013.3	-	6293.5	-	6928.2	-
OE[34]	5782.2	1.2	6018.3	0.08	4968.3	−21.06	6399.6	−7.63
OEP[35]	5872.6	2.78	6793.5	12.97	5859.3	−6.9	6926.1	−0.03
DS	**6224.1**	**8.93**	**7134.1**	**18.64**	**6346.3**	**0.84**	**7316.3**	**5.6**

Note: The bold values indicate the highest GMP of the proposed DS configuration.

- The proposed DS method eliminates the limitations of population-based meta-heuristic optimization algorithms,[7,10,11,13] including high search domain, convergence problems, parameter shortlisting-related aspects, complex and lengthy procedures, getting trapped at the local optimal solution, weighting component selection constraints, gigantic calculations, large computational time, etc.

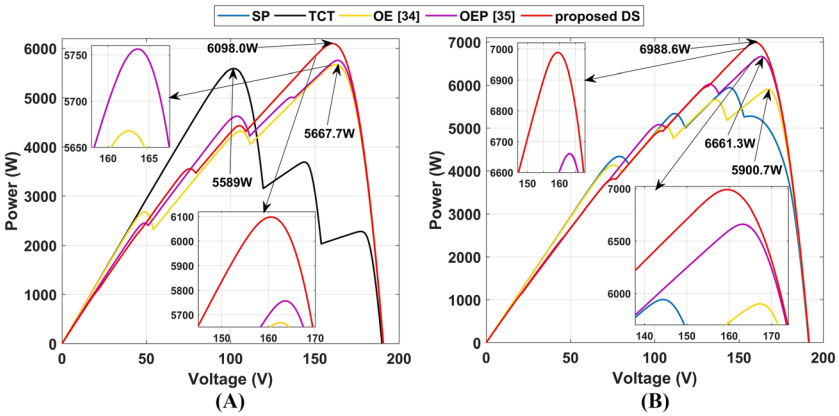

FIGURE 31 PV characteristics of a 8 × 6 PV array for 30°C temperature under (A) case-23 and (B) case-24

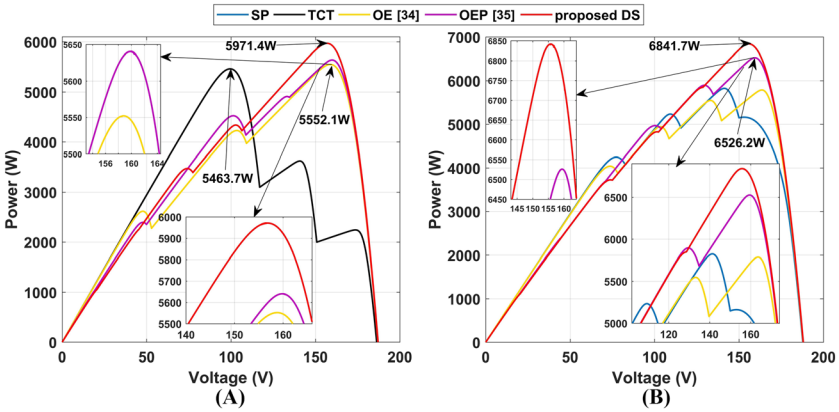

FIGURE 32 PV characteristics of a 8 × 6 PV array for 35°C temperature under (A) case-23 and (B) case-24

TABLE 9 GMP (in watt) of a 6 × 8 PV array for 30°C and 35°C temperatures

	Case-23				Case-24			
	T = 30°C		T = 35°C		T = 30°C		T = 35°C	
Config.	GMP	FF	GMP	FF	GMP	FF	GMP	FF
SP	5589.0	0.495	5463.8	0.492	5941.5	0.526	5824.9	0.525
TCT	5589.0	0.495	5463.7	0.492	5900.7	0.523	5786.9	0.521
OE[34]	5667.7	0.502	5552.1	0.500	5900.7	0.523	5786.9	0.521
OEP[35]	5756.2	0.548	5640.7	0.546	6661.3	0.616	6526.2	0.614
DS	**6098.0**	**0.598**	**5971.4**	**0.596**	**6988.6**	**0.646**	**6841.7**	**0.643**

Note: The bold values indicate the highest GMP of the proposed DS configuration.

- A majority of the recently reported static reconfiguration techniques[14–26,28–33] fail to be compatible with all sizes of PV arrays. Hence, they are not scalable and generalized.
- Despite its better technical performance compared to the conventional SP and TCT configurations, the existing CB technique[26] suffers from this major limitation as it cannot be applicable to the nonsymmetrical sizes of PV arrays. In contrast, the proposed DS technique is compatible with all symmetrical and nonsymmetrical PV array sizes and further shows its superior performance in generating more power compared to CB.

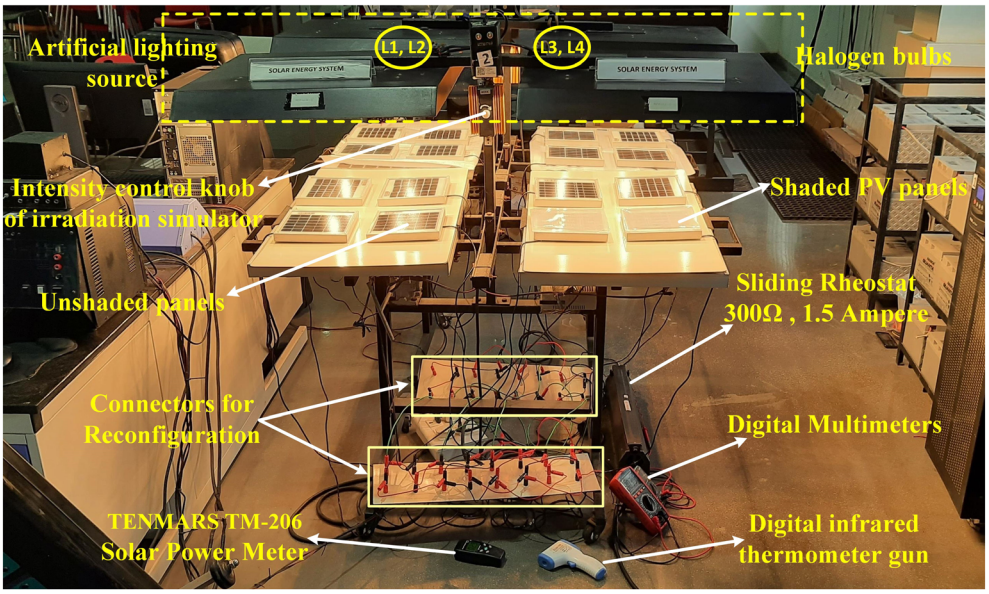

FIGURE 33 Laboratory test setup for experimental validation

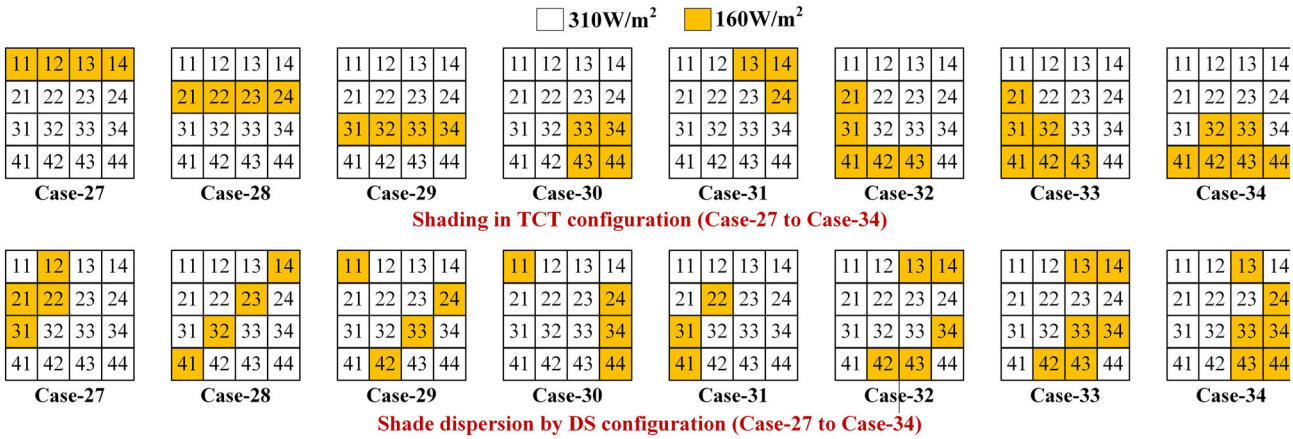

FIGURE 34 Shading in TCT and DS configurations under case-27 to case-34

TABLE 10 Experimental and simulation results of power output of TCT and DS configurations

	Power output (W)			
	TCT configuration		DS configuration	
Shading case	Experimental	Simulation	Experimental	Simulation
Case-27	8.40	8.3322	12.58	11.6924
Case-28	8.40	8.3322	13.83	12.6280
Case-29	8.40	8.3322	13.83	12.6280
Case-30	11.95	11.443	13.83	12.6280
Case-31	12.62	11.790	13.93	12.8001
Case-32	10.63	10.071	12.42	11.3501
Case-33	10.52	9.9582	11.85	11.0787
Case-34	8.33	8.2443	12.50	11.2481

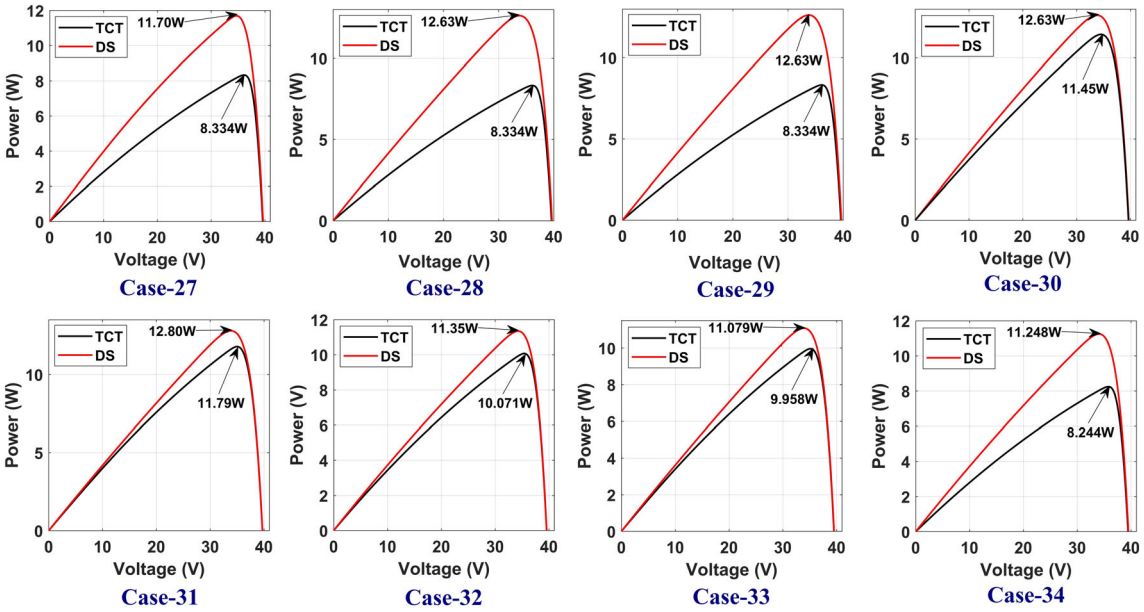

FIGURE 35 Simulation results: PV characteristics under case-27 to 34

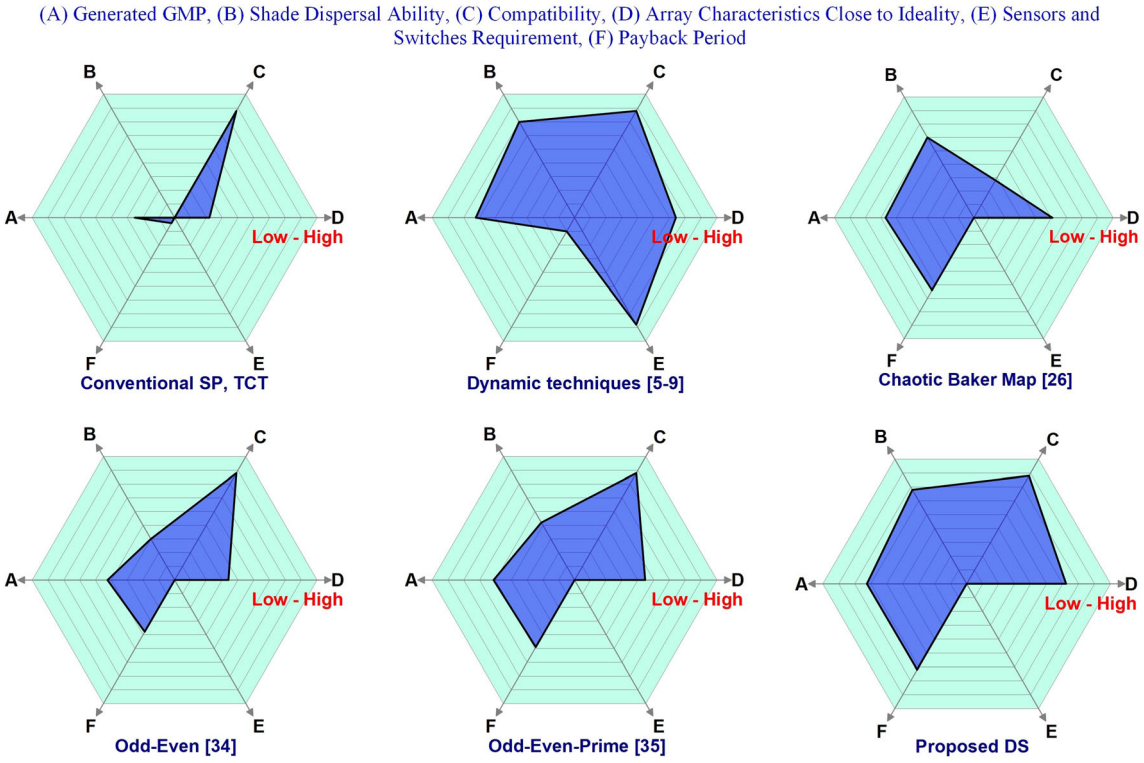

FIGURE 36 Wheel chart depicting the performance of various reconfiguration approaches

- The recently reported OE[34] and OEP[35] techniques despite being applicable to any sizing of PV array, significantly fail to disperse the effect over the entire array in order to mitigate the mismatch between rows under PS. Due to their ineffective shade dispersion, the array characteristics are considerably distorted making the task highly challenging for MPPT controllers to track the global maximum power point (GMPP). On contrary, the DS technique disperses the shade effectively and also exhibits comparatively smoother characteristics closer to the ideal characteristics reducing the burden on MPPT systems.

The qualitative comparison of different aspects of the various configurations with the proposed DS is explained in the wheel chart as shown in Figure 36.

6.6 | Economic analysis

Under normal conditions, the considered 8 × 8 PV array generates 81,074 units/day. But, under different PS conditions, the array output is reduced due to mismatch losses. This reduction in output can be mitigated to the most possible extent by using the proposed DS method. The electricity units and the respective revenue generation are evaluated to show the effectiveness of the proposed configuration. Generally, under normal days, the PV array works efficiently during peak sun hours. So, for investigation, the aforementioned shading cases 1 to 6 are considered to take place over the array each hour from 9 a.m. to 4 p.m. The tariff of ₹4 (INR) per unit is regarded for estimation. A detailed comparative economic analysis of TCT, CB, and DS configurations under various shading cases is shown in Table 11.

From the table, it is noted that the TCT, CB, and DS configurations generate 18,169.62, 19,864.35, and 21,168.54 units per year, respectively. The respective revenue generated per year is ₹72,678.5 (INR), ₹79,457.43 (INR), and ₹84,674.16 (INR). By employing the proposed DS configuration, the respective units and the revenue generation are increased by 2998.92kWh and ₹11,995.67 (INR) which is nearly 16.51% more than the standard TCT. Whereas the existing CB yields the percentage enhancement of only 9.32% in the units and revenue generated when compared to TCT. Further, it is noted from Table 11 that it is exemplary to confirm that the proposed DS technique yields higher economic benefits than the other configurations under PS. By enlarging the ratings of the panels, the output can be

TABLE 11 A comparative economic analysis of various configurations of 8 × 8 array under various PS conditions

				Hourly		Daily		Yearly	
Array Config	**Hour**	**Shade case**	**GMP (W)**	**Units/h (kWh)**	**Revenue/h (INR)**	**Units/day (kWh)**	**Revenue/day (INR)**	**Units/year (kWh)**	**Revenue/year (INR)**
TCT	9–10	1	7122.8	7.1228	28.4912	49.7798	199.1192	18,169.627	72,678.508
	10–11	2	7122.7	7.1227	28.4908				
	11–12	3	8750.2	8.7502	35.0008				
	12–1	4	5567.1	5.5671	22.2684				
	1–2	5	8313.0	8.3130	33.252				
	2–3	6	6452.0	6.4520	25.808				
	3–4	6	6452.0	6.4520	25.808				
CB [26]	9–10	1	7536.3	7.5363	30.1452	54.4229	217.6916	19,864.358	79,457.434
	10–11	2	7137.4	7.1374	28.5496				
	11–12	3	9369.1	9.3691	37.4764				
	12–1	4	6262.5	6.2625	25.05				
	1–2	5	9670.2	9.6702	38.6808				
	2–3	6	7223.7	7.2237	28.8948				
	3–4	6	7223.7	7.2237	28.8948				
DS	9–10	1	7504.1	7.5041	30.0164	**57.996**	**231.984**	**21,168.54**	**84,674.161**
	10–11	2	7980.0	7.9800	31.92				
	11–12	3	9497.0	9.4970	37.988				
	12–1	4	6702.0	6.7020	26.808				
	1–2	5	9793.1	9.7931	39.1724				
	2–3	6	8259.9	8.2599	33.0396				
	3–4	6	8259.9	8.2599	33.0396				

Note: The bold values indicate the highest values obtained for the proposed DS configuration.

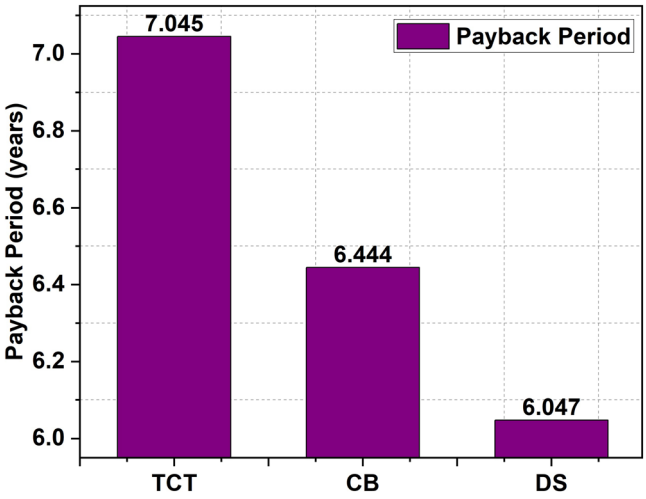

FIGURE 37 Payback period of various configurations

augmented and thus maximizing the generated revenue. The payback period is also reduced significantly with the proposed technique as shown in Figure 37.

7 | CONCLUSIONS

In this paper, a highly efficient calligraphy-based DS method is proposed for effective shade dispersal in the Partially Shaded PV Arrays. The proposed DS configuration outperformed standard SP, TCT, existing image processing Chaotic Baker Map,[26] Odd-Even,[34] Odd-Even-Prime[35] based configurations by effectively dispersing the shade over the entire array thereby enhancing the PV array row currents and mitigating the mismatch between them. To validate the compatibility and efficacy of the proposed configuration, the system is tested for various symmetrical and unsymmetrical sizes such as 9×9, 8×8, 4×4, 8×6 PV arrays under 34 distinct shading cases and extensively analyzed with eight performance indices. Further, the variation in temperature by $\pm 5^{\circ}C$ is also considered in simulation studies. To experimentally validate the proposed configuration, a laboratory experimental setup of a 4×4 PV array reconfiguration system is developed and tested under eight distinct conditions. Besides overcoming the drawbacks of existing configurations, the proposed DS configuration enhances the GMP by a significant percentage and further exhibits consistent and superior performance with improved values of Y_A, FF, efficiency, CF, PR during all the shading cases. However, the existing configurations offer an inferior and inconsistent performance. Due to the effective shade dispersal of the proposed DS method, the mismatch losses are significantly reduced and hence exhibit comparatively smoother array characteristics. When compared to both TCT and CB configurations of an 8×8 PV array, the corresponding revenue generated is increased by 16.51% and 6.57% with the employment of proposed DS configuration. So, it is commendable to confirm that the proposed method effectively disperses the shade over the entire array and is quite suitable to be executed under shading conditions.

DATA AVAILABILITY STATEMENT

Data sharing is not applicable to this article as no new data were created or analyzed in this study.

ORCID

Rayappa David Amar Raj https://orcid.org/0000-0002-5888-5513

REFERENCES

1. Solórzano J, Egido MA. Hot-spot mitigation in PV arrays with distributed MPPT (DMPPT). *Sol Energy*. 2014;101:131-137. doi:10.1016/j.solener.2013.12.020
2. Raj RDA, Naik KA. A novel solar photovoltaic array reconfiguration technique using two-dimensional generalized Arnold's cat map. *J Sol Energy Eng*. 2022;144(6):061001. doi:10.1115/1.4054506

3. Kumari N, Shiva Kumar S, Laxmi V. Design of an efficient bipolar converter with fast MPPT algorithm for DC nanogrid application. *Int J Circuit Theory Appl*. 2021;49(9):3162-3174. doi:10.1002/cta.3020
4. Sai Krishna G, Moger T. Reconfiguration strategies for reducing partial shading effects in photovoltaic arrays: state of the art. *Sol Energy*. 2019;182:429-452. doi:10.1016/j.solener.2019.02.057
5. Varma GHK, Barry VR, Jain RK, Kumar D. An MMTES algorithm for dynamic photovoltaic array reconfiguration to enhance power output under partial shading conditions. *IET Renew Power Gener*. 2021;15(4):809-820. doi:10.1049/rpg2.12070
6. Karmakar BK, Karmakar G. A current supported PV Array reconfiguration technique to mitigate partial shading. *IEEE Trans Sustain Energy*. 2021;12(2):1449-1460. doi:10.1109/TSTE.2021.3049720
7. Babu TS, Ram JP, Dragičević T, Miyatake M, Blaabjerg F, Rajasekar N. Particle swarm optimization based solar PV array reconfiguration of the maximum power extraction under partial shading conditions. *IEEE trans Sustain Energy*. 2018;9(1):74-85. doi:10.1109/TSTE.2017.2714905
8. Sanseverino ER, Ngoc TN, Cardinale M, et al. Dynamic programming and Munkres algorithm for optimal photovoltaic arrays reconfiguration. *Solar Energy*. 2015;122:347-358. doi:10.1016/j.solener.2015.09.016
9. Bouselham L, Rabhi A, Hajji B, Mellit A. Photovoltaic array reconfiguration method based on fuzzy logic and recursive least squares: an experimental validation. *Energy*. 2021;232:121107. doi:10.1016/j.energy.2021.121107
10. Zhang X, Li C, Li Z, et al. Optimal mileage-based PV array reconfiguration using swarm reinforcement learning. *Energ Conver Manage*. 2021;232:113892. doi:10.1016/j.enconman.2021.113892
11. Yang B, Shao R, Zhang M, et al. Socio-inspired democratic political algorithm for optimal PV array reconfiguration to mitigate partial shading. *Sustain Energy Technol Assess*. 2021;48:101627. doi:10.1016/j.seta.2021.101627
12. Yadav VK, Yadav A, Yadav R, et al. A novel reconfiguration technique for improvement of PV reliability. *Renew Energy*. 2022;182:508-520. doi:10.1016/j.renene.2021.10.043
13. Ajmal AM, Ramachandaramurthy VK, Naderipour A, Ekanayake JB. Comparative analysis of two-step GA-based PV array reconfiguration technique and other reconfiguration techniques. *Energy Conv And Manage*. 2021;230:113806. doi:10.1016/j.enconman.2020.113806
14. Rani BI, Ilango GS, Nagamani C. Enhanced power generation from PV array under partial shading conditions by shade dispersion using Su Do Ku configuration. *IEEE Trans Sustain Energy*. 2013;4(3):594-601. doi:10.1109/TSTE.2012.2230033
15. Krishna SG, Moger T. Optimal SuDoKu reconfiguration technique for total-cross-tied PV array to increase power output under non-uniform irradiance. *IEEE Trans Energy Conv*. 2019;34(4):1973-1984. doi:10.1109/TEC.2019.2921625
16. Tatabhatla VMR, Agarwal A, Kanumuri T. Performance enhancement by shade dispersion of solar photo-voltaic array under continuous dynamic partial shading conditions. *J Clean Prod*. 2019;213:462-479. doi:10.1016/j.jclepro.2018.11.015
17. Satpathy PR, Sharma R, Jena S. A shade dispersion interconnection scheme for partially shaded modules in a solar PV array network. *Energy*. 2017;139:350-365. doi:10.1016/j.energy.2017.07.161
18. Satpathy PR, Sharma R. Power loss reduction in partially shaded PV arrays by a static SDP technique. *Energy*. 2018;156:569-585. doi:10.1016/j.energy.2018.05.131
19. Belhaouas N, Cheikh MSA, Agathoklis P, et al. PV array power output maximization under partial shading using new shifted PV array arrangements. *Appl Energy*. 2017;187:326-337. doi:10.1016/j.apenergy.2016.11.038
20. Venkateswari R, Rajasekar N. Power enhancement of PV system via physical array reconfiguration based Lo Shu technique. *Energ Conver Manage*. 2020;215:112885. doi:10.1016/j.enconman.2020.112885
21. Dhanalakshmi B, Rajasekar N. A novel competence square based PV array reconfiguration technique for solar PV maximum power extraction. *Energ Conver Manage*. 2018;174:897-912. doi:10.1016/j.enconman.2018.08.077
22. Ramesh T, Rajani K, Panda AK. A novel triple-tied-cross-linked PV array configuration with reduced number of cross-ties to extract maximum power under partial shading conditions. *CSEE J Power Energy Systems*. 2021;7(3):567-581. doi:10.17775/CSEEJPES.2020.00750
23. Madhanmohan VP, Nandakumar M, Saleem A. Enhanced performance of partially shaded photovoltaic arrays using diagonally dispersed total cross tied configuration. *Energy Sources Part a: Recovery Util Environ Effect*. 2020;1-19. doi:10.1080/15567036.2020.1826008
24. Satpathy PR, Sharma R. Power and mismatch losses mitigation by a fixed electrical reconfiguration technique for partially shaded photovoltaic arrays. *Energ Conver Manage*. 2019;192:52-70. doi:10.1016/j.enconman.2019.04.039
25. Sreekantha Reddy S, Yammani C. A novel magic-square puzzle based one-time PV reconfiguration technique to mitigate mismatch power loss under various partial shading conditions. *Optik*. 2020;222:165289. doi:10.1016/j.ijleo.2020.165289
26. Tatabhatla VMR, Agarwal A, Kanumuri T. A generalized chaotic baker map configuration for reducing the power loss under shading conditions. *Electr Eng*. 2020;102(4):2227-2244. doi:10.1007/s00202-020-01016-4
27. Satpathy PR, Babu TS, Shanmugam SK, Popavath LN, Alhelou HH. Impact of uneven shading by neighboring buildings and clouds on the conventional and hybrid configurations of roof-top PV arrays. *IEEE Access*. 2021;9:139059-139073. doi:10.1109/ACCESS.2021.3118357
28. Rajani K, Ramesh T. Maximum power enhancement under partial shadings using a modified Sudoku reconfiguration. *CSEE J Power Energy Syst*. 2021;7(6):1187-1201. doi:10.17775/CSEEJPES.2020.01100
29. Kumar Pachauri R, Thanikanti SB, Bai J, et al. Ancient Chinese magic square-based PV array reconfiguration methodology to reduce power loss under partial shading conditions. *Energ Conver Manage*. 2022;253:115148. doi:10.1016/j.enconman.2021.115148

30. Ye C, Tai C, Huang Y, Chen J. Dispersed partial shading effect and reduced power loss in a PV array using a complementary SuDoKu puzzle topology. *Energ Conver Manage*. 2021;246:114675. doi:10.1016/j.enconman.2021.114675
31. Anjum S, Mukherjee V, Mehta G. Modelling and simulation of AdDoKu based reconfiguration technique to harvest maximum power from photovoltaic array under partial shading conditions. *Simul Model Pract Theory*. 2022;115:102447. doi:10.1016/j.simpat.2021.102447
32. Rakesh N, Kumar SS, Madhusudanan G. Mitigation of power mismatch losses and wiring line losses of partially shaded solar PV array using improvised magic technique. *IET Renew Power Gener*. 2019;13(9):1522-1532. doi:10.1049/iet-rpg.2018.5927
33. Anjum S, Mukherjee V. A novel arithmetic sequence pattern reconfiguration technique for line loss reduction of photovoltaic array under non-uniform irradiance. *J Clean Prod*. 2022;331:129822. doi:10.1016/j.jclepro.2021.129822
34. Yadav K, Kumar B, Swaroop D. Mitigation of mismatch power losses of PV array under partial shading condition using novel odd even configuration. *Energy Rep*. 2020;6:427-437. doi:10.1016/j.egyr.2020.01.012
35. Reddy SS, Yammani C. Odd-even-prime pattern for PV array to increase power output under partial shading conditions. *Energy*. 2020; 213:118780. doi:10.1016/j.energy.2020.118780
36. Rezazadeh S, Moradzadeh A, Hashemzadeh SM, Pourhossein K, Mohammadi-Ivatloo B, Hosseini SH. A novel prime numbers-based PV array reconfiguration solution to produce maximum energy under partial shade conditions. *Sustain Energy Technol Assess*. 2021;47: 101498. doi:10.1016/j.seta.2021.101498
37. Raj RDA, Naik KA. Optimal reconfiguration of PV array based on digital image encryption algorithm: a comprehensive simulation and experimental investigation. *Energ Conver Manage*. 2022;261:115666. doi:10.1016/j.enconman.2022.115666
38. Satpathy PR, Jena S, Sharma R. Power enhancement from partially shaded modules of solar PV arrays through various interconnections among modules. *Energy*. 2018;144:839-850. doi:10.1016/j.energy.2017.12.090
39. Satpathy PR, Sharma R, Dash S. An efficient SD-PAR technique for maximum power generation from modules of partially shaded PV arrays. *Energy*. 2019;175:182-194. doi:10.1016/j.energy.2019.03.078
40. Amar Raj RD, Anil Naik K. An image encryption concept based solar photovoltaic array reconfiguration techniques for mismatch mitigation. *Energy Sources Part a: Recovery Util Environ Effect*. 2022;44(1):951-972. doi:10.1080/15567036.2022.2052383
41. Maniccam SS, Bourbakis NG. Image and video encryption using SCAN patterns. *Pattern Recogn*. 2004;37(4):725-737. doi:10.1016/j.patcog.2003.08.011
42. Dong W, Li Q, Tang Y. Image encryption-then-transmission combining random sub-block scrambling and loop DNA algorithm in an optical chaotic system. *Chaos Soliton Fract*. 2021;153:111539. doi:10.1016/j.chaos.2021.111539
43. https://www.sciencedirect.com/topics/social-sciences/calligraphy
44. https://docs.microsoft.com/en-us/typography/font-list/edwardian-script-itc
45. Yousri D, Allam D, Eteiba MB. Optimal photovoltaic array reconfiguration for alleviating the partial shading influence based on a modified Harris hawks optimizer. *Energ Conver Manage*. 2020;206:112470. doi:10.1016/j.enconman.2020.112470
46. Amar Raj RD, Anil Naik K. A generalized Henon map-based solar PV Array reconfiguration technique for power augmentation and mismatch mitigation. *IETE J Res*. 2022;1-19. doi:10.1080/03772063.2022.2055660

How to cite this article: Raj RDA, Naik KA. A novel scan pattern for reconfiguration of partially shaded photovoltaic arrays for maximum power extraction. *Int J Circ Theor Appl*. 2023;51(2):668-701. doi:10.1002/cta.3452